Bollettino di Geofisica Teorica ed Applicata Vol. 58, n. 1, pp. 17-42; March 2017
DOI 10.4430/bgta0191

Local earthquake tomography of Izmir geothermal area, Aegean region of Turkey

C. Ozer[1,2,3] and O. Polat[1]

[1] *Department of Geophysics, Engineering Faculty, Dokuz Eylul University, Izmir, Turkey*
[2] *The Institute of Natural and Applied Sciences, Dokuz Eylul University, Izmir, Turkey*
[3] *Department of Geophysics, Oltu Earth Sciences Faculty, Ataturk University, Erzurum, Turkey*

(Received: March 13, 2017; accepted: April 27, 2017)

ABSTRACT The Izmir Gulf and surrounding areas are located within an important geothermal area of Turkey in the Aegean region (western Anatolia). The region represents a natural laboratory where multi-disciplinary approaches in Earth sciences find a venue for the study of the dynamics of the coupled lithosphere-fault system. Seismological studies are being carried out to investigate the origin and the nature of the Earth structure. In the present study, we perform a first attempt to define the crust and upper mantle seismic properties using local earthquake tomography. The major tectonic features within the 170×90 km^2 rectangular area include the Aliaga, Balcova, Menemen, and Seferihisar geothermal systems and the Urla hot spring. 783 well-located earthquakes, each one with at least 11 travel time readings, are selected to assemble a bulk of 7676 P-phase and 6431 S-phase picks. The 3D distribution of P-wave velocity (V_p), S-wave velocity (V_s), and the P-wave/S-wave velocity ratio (V_p/V_s) allows a resolution of the Earth crust down to 30 km of depth. The thickest and broadest low-V_p velocity anomalies are found beneath the Outer Gulf and north of Izmir Bay. A high V_p/V_s ratio corresponding to a low-V_s model is detected beneath the Menemen geothermal system. From local tomography, we identify four main seismic layers at variable depths from the surface to the lower crust. The lower crust/mantle discontinuity is found at approximately 27 km of depth. This transition is characterized by an undulated shape, and intrusive bodies are imaged beneath the main geothermal systems.

Key words: seismic crustal structure, local earthquake tomography, Izmir, Aegean region of Turkey, western Anatolia.

1. Introduction

The Aegean region of Turkey, known as one of the most seismically active areas in the eastern Mediterranean region, attracts ongoing attention as it includes a broad area of distributed deformation characterized by a N-S extensional tectonic regime. This system creates E-W-trending grabens with intervening horsts and associated normal faults that developed since the Upper Miocene-Pliocene (Reilinger *et al*., 2010; Yin, 2010; Oner and Dilek, 2011; Jolivet *et al*., 2013). Since major earthquakes occur mainly along the North Anatolian Fault (NAF) zone (Fig. 1), most seismological studies have focused on determining seismicity and estimating the seismic

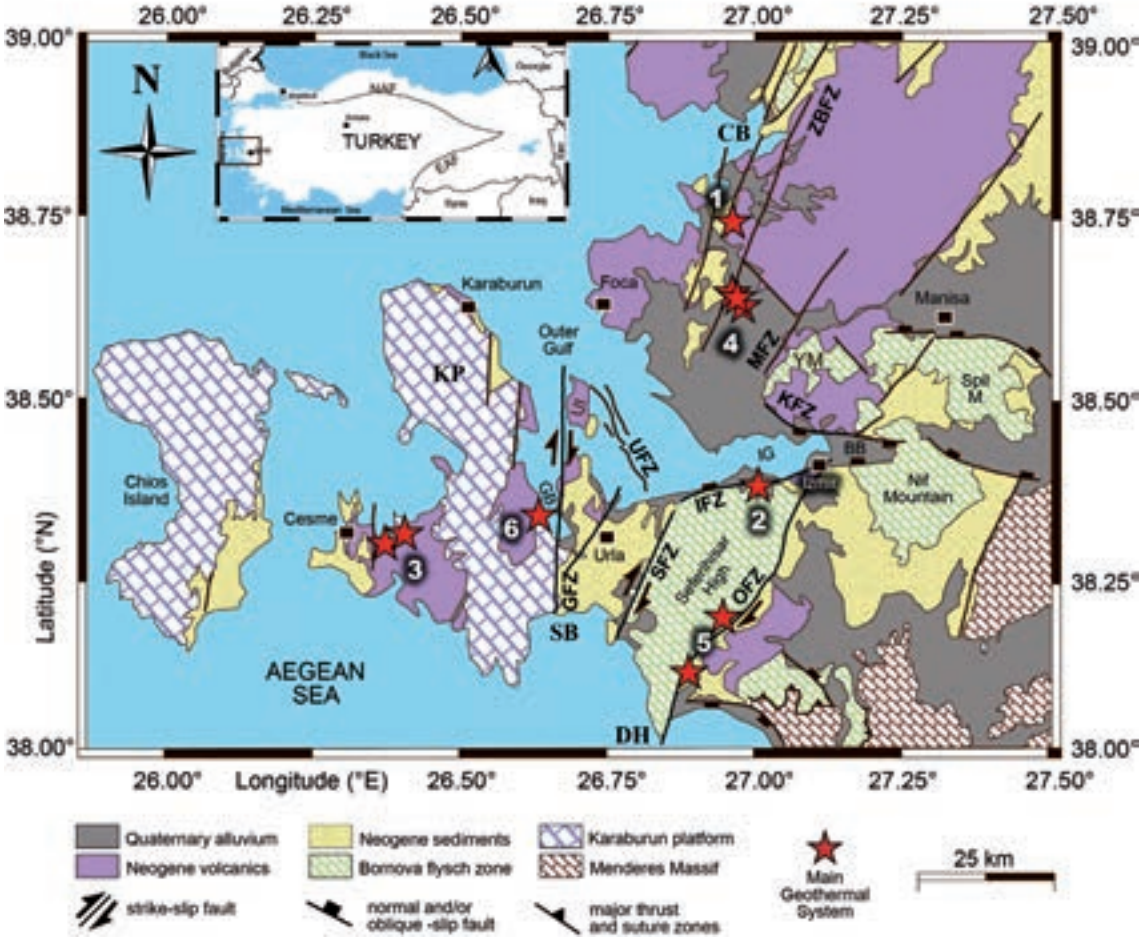

Fig. 1 - Geological map and principal tectonic features around the Izmir geothermal area. Abbreviations; BB: Bornova Basin; CB: Candarli Bay, DH: Doganbey Horn, GB: Gulbahce Bay, GFZ: Gulbahce Fault zone, IG: Inner Bay of the Izmir Gulf, IFZ: Izmir Fault zone, KFZ: Karsiyaka Fault zone, KP: Karaburun peninsula, MFZ: Menemen Fault zone, OFZ: Orhanli Fault zone, SB: Sigacik Bay, SFZ: Seferihisar Fault zone, UI: Uzunada Island, UFZ: Uzunada Fault zone, YM: Yamanlar mountain, ZBFZ: Zeytindag-Bergam Fault zone. Main geothermal systems; 1: Aliaga-AGS, 2: Balcova-BGS, 3: Cesme-CGS, 4: Menemen-MGS, 5: Seferihisar-SGS, 6: Urla-UHS. Inset map: NAF: North Anatolian Fault, EAF: East Anatolian Fault (modified after Emre and Ozalp, 2011; Uzel *et al*., 2012; Erkan, 2015; Coskun *et al*., 2016).

hazard for the western Anatolia, the Marmara, and the Aegean regions (e.g., Gurbuz *et al*., 2000, 2003; Polat *et al*., 2002a, 2002b, 2008; Cisternas *et al*., 2004; Tunc, 2008; Tunc *et al*., 2011; Gok and Polat, 2012; Avsar *et al*., 2014a, 2014b, 2015, 2016; Frederiksen *et al*., 2015; Kahraman *et al*., 2015; Poyraz *et al*., 2015; Ozmen and Can, 2016; Ozer and Polat, 2017).

In this paper, local earthquakes are studied for the first time to investigate the seismic velocity structure of the complex Izmir area. While additional applications such as teleseismic and ambient noise tomography could improve the resolution of the rheologic/structural features and decrease uncertainties in tomography, it is also possible to investigate the study area using a dense seismic array (Xu *et al*., 2009; Sufri *et al*., 2016). This experiment took place around the periphery of the Izmir geothermal area located at the western extremity of the Aegean region (western Anatolia).

This area is characterized by elevated heat flow values of 95 mW/m concentrated mainly along the coastal areas including Izmir (e.g., Ilkisik, 1995; Dolmaz *et al*., 2005; Salk *et al*., 2005; Akin *et al*., 2014; Bilim *et al*., 2016). Interpretation of gravity and aeromagnetic anomalies in Izmir and surroundings found isostatically thickened crust which increases in thickness towards the east (Ates *et al*., 1999). Magnetotelluric measurements revealed resistivity patterns associated with the main tectonic features. The findings exhibit low resistivity along the basins and grabens down to 5 km of depth, indicating complex tectonic structures (e.g., Ozguler and Unay, 1977; Caglar, 2001; Gurer *et al*., 2004; Kaya, 2010). No dense arrays of seismic stations were deployed in the past within the Izmir region. However, some studies reported significant velocity anomalies beneath Anatolia and a decrease in crustal thickness north and NW of Turkey (e.g., Gurbuz *et al*., 2003; Bekler and Gurbuz, 2008). Coskun *et al*. (2016) performed a marine geophysical study revealing the submarine sea-bottom morphology by acoustic data. They found a fault zone mainly aligned in the NW-SE direction in the Gulf of Izmir. Another study in the Izmir Gulf was conducted to investigate the coseismic displacements of the October 17-21, 2005 (*M* 5.9) Izmir earthquake that caused extensive damage (Pamukcu *et al*., 2015a). Other detailed investigations of vertical and horizontal deformations were performed by monitoring microgravity and GPS/GNSS methods (e.g., Aktug and Kilicoglu, 2006; Pamukcu and Yurdakul, 2008; Ozener *et al*., 2013; Pamukcu *et al*., 2015b).

From these studies, it has been suggested that earthquake locations play a significant role in seismological and seismotectonic interpretations and in evaluating scenarios for settlement areas (Gok *et al*., 2014). These evaluations can only be achieved if velocity structure and deformation characteristics are accurately and precisely known. Many tomographic studies depending heavily on the number of used stations, methods, data amount, and ray path density, reported a crustal thickness ranging from 20 to 35 km, and an almost flat crust-mantle transition beneath central Anatolia (e.g., Salah *et al*., 2007, 2014; Cambaz and Karabulut, 2010; Tezel *et al*., 2010; Bakirci *et al*., 2012; Salaun *et al*., 2012). Other studies on attenuation and anisotropy, have shown an agreement in anisotropy directions between Pn and Sn waves, highlighting an extensional component towards the southern Aegean Sea (e.g., Mutlu and Karabulut, 2011; Sahin *et al*., 2013; Paul *et al*., 2014; Sahin and Cinar, 2014). Very few seismological studies have been carried out in the study area. One of the recent attempts was performed by using ambient noise tomography and presented a poor understanding of the complex subsurface structures due to the lack of a denser seismic array (Delph *et al*., 2015). High resolution and accurate crustal imaging from local earthquake tomography (LET) has never been applied in the Izmir area. Previous seismological studies display some estimates of crustal thickness based on sparse distributions of temporary and permanent seismic stations (Salah *et al*., 2007; Tezel *et al*., 2010; Salaun *et al*., 2012; Karabulut *et al*., 2013).

The LET algorithm is often preferred in many studies since it reveals crustal seismic variations by performing 3-D joint inversion for hypocentral parameters and velocities. The velocity perturbations have close relations with lithological changes, petrological characteristics of rocks, fluid-rich and high-pore-pressure sub-areas, regional tectonics, and the structure and geometry of faults (Koulakov *et al*., 2009, 2010a, 2010b; Kaypak and Gokkaya, 2012, Muksin *et al*., 2013). The algorithm represents a useful and convenient tool to reconstruct the regional tectonics and seismogenic characteristics. The Earthquake Department of the Disaster and Emergency Management Authority (AFAD) has greatly enhanced earthquake monitoring capability in Turkey since 2005 by deploying new seismic stations (Inan *et al*., 2007; Polat *et al*., 2009).

2. Geology, tectonics and hydrothermal activities

The geological structure of the Izmir area is formed by six principal units (Fig. 1) that have a relation with the deformation, regime, extensional tectonics, and basin formation. The Menderes Massif is a well-defined core complex of western Anatolia (Gessner *et al.*, 2001). The Karaburun Platform is mainly observable along the N-S direction in the Karaburun Peninsula (KP) and is composed of Palaeozoic-Mesozoic carbonate platforms in the west of the study area. It is characterized by andesitic to rhyolitic and felsic pyroclastic rocks. All of these units are overlain with Urla Neogene sediments. These overlying units are reported as Middle Miocene in age (Genc *et al.*, 2001; Ersoy *et al.*, 2014). The Bornova flysch zone covers a wide area and is assumed as the basement unit in the study area. It comprises limestones, cherts, submarine volcanic rocks and serpentinites embedded in a flysch-type sedimentary matrix with a metamorphic grade representing Yamanlar Mountain (YM) to the north, Spil Mountain (SM) to the NE, Nif Mountain (NM) to the east and the Seferihisar High (SH) to the south of the Gulf of Izmir (Uzel *et al.*, 2012). Neogene volcanic rocks are mainly oriented in the E-W and NE-SW directions overlying the Bornova flysch zone. Foca volcanic rocks to the north of the study area are represented by a lower and an upper succession. They overlie the alluvial fan and fluvio-lacustrine sedimentary units of the lower sedimentary succession. The upper sedimentary succession, represented largely by lacustrine limestones and underlying sandstones, is intercalated with and conformably overlain by the mafic rocks (Okay and Altiner, 2007; Ersoy *et al.*, 2014). Quaternary alluvium is characterized by the E-W to NW-SE trending Izmir Bay filled with Plio-Quaternary alluvial fan and shallow marine sediments. The Bornova Basin (BB) to the east and northern parts and a very narrow strip oriented in the E-W direction along the southern coast of the Gulf of Izmir are filled with this young sedimentary deposit (Uzel *et al.*, 2013). The Aegean region in Turkey is geographically well known for its numerous gulfs, such as Candarli Bay (CB) located to the north, Izmir Bay in the middle, and Sigacik Bay (SB) to the south of the study area. Izmir Bay is one of the most distinctive bays in the region, having an L-shaped basin controlled by active faults. It can be divided into two basins, based on their surface and subsurface morphology: Inner and Outer gulfs. The Outer Gulf is divided by another depression named Gulbahce Bay (GB).

The orientation of the main faults is NE-SW, N-S, NW-SE and E-W. Two fault zones, named the Seferihisar (SFZ), and Orhanli fault zones (OFZ) with NE-SW orientation, bound the SH from the western and eastern parts of the Aegean Sea and the Gulf of Izmir. The SFZ is a dextral fault zone 2-5 km wide and 30 km long. Towards the north, the fault bends to N40-50°E (Uzel *et al.*, 2013) and links with the Izmir Fault Zone (IFZ). The OFZ is the most prominent structure in the region and is located SW of Izmir. It bounds the SH to the east and can be traced for approximately 45 km from the Gulf of Izmir to the Doganbey Horn (DH) to the south. Other main tectonic features located at the northern part of the study area are the Menemen (MFZ) and Zeytindag-Bergama (ZBFZ) fault zones. The N-S trending Gulbahce Fault Zone (GFZ) can be followed between GB and SB bounding KP and Urla Neogene sediments. Surface rupture during the October 17-21, 2005 (M5.9) earthquake started as dextral from the SB and ended as an oblique-reverse fault towards the GB (Emre and Ozalp, 2011). The NW-SE trending fault named Uzunada Fault Zone (UFZ) was recently investigated by marine geophysical studies and interpreted as a feature 15 km long and 2 km wide along the Outer Gulf to the east of the Uzunada Island (UI) (Coskun *et al.*, 2016). The UFZ shows some normal faults trending in the NW-SE

direction detected from the seabed topography (Fig. 1). The IFZ extends along the southern coast of the IG. It is an E-W trending active normal fault zone approximately 2-4 km wide and 40 km long. It bounds the SH and NM. The northern part of the Inner Bay is bounded by the Karsiyaka Fault zone (KFZ), which is an antithetic fault of the IFZ. It is also a normal fault zone 0.5-2.5 km wide and 20 km long (Uzel *et al*., 2012).

The Aegean region of Turkey lies in an important geothermal energy zone along the active Alpine-Himalayan Orogenic Belt. Western Anatolia has more than 600 hot springs, with temperatures ranging from 25°C to as high as 287°C in hydrothermal alteration zones. However, some important resources are located in the study area (Aksoy *et al*., 2008). Because hydrothermal manifestations are spread throughout the study area, the geothermal resources of Izmir and its surroundings reveal a high potential to implement energy and balneological facilities. The study area includes six principal geothermal areas around the Gulf of Izmir, oriented mainly in N-S and E-W directions. These resources are 1) AGS-Aliaga geothermal system, 2) BGS-Balcova geothermal system, 3) CGS-Cesme geothermal system, 4) MGS-Menemen geothermal system, 5) SGS-Seferihisar geothermal system, 6) UHS-Urla hot spring, with temperatures of 98, 140, 56-62, 55, 56-95, and 19-32 °C, respectively (Yilmazer and Alacali, 2005). The hydrothermal patterns of the geothermal resources are strongly controlled by the NE-SW, N-S, and E-W oriented fault zones (Fig. 1). The IFZ, GFZ, OFZ, and ZBFZ are responsible for several geothermal areas by providing effective conduits for the geothermal systems in the study area. The AGS and MGS are located in an area of faults. The BGS is in the E-W trending IFZ, located at the SH. It is limited to the narrow, nearly vertical zone where the Bornova flysch deposits appear to be fragmented by faults. The CGS of the western extremity of the Karaburun Peninsula discharges mainly from Neogene volcanics. The SGS developed over the OFZ, which bounds horst and graben structures. The UHS has some outflows of hot water resources near GB, but there is no detailed research regarding geothermal energy to reveal its potential. It has a flow rate of 10 l/s (Serpen *et al*., 2009; Magri *et al*., 2010).

3. Data, algorithm, and test

3.1. Background of data

It should be noted that data quality varies according to the station equipment, deploying time, conditions at station sites, and earthquake magnitude. The permanent seismic network in Izmir and the surrounding area consists of 44 stations in total (Fig. 2). The recording period goes from the middle of August 2008 until the end of December 2014. Most of the stations (~60%) were operated by the AFAD and collected at least three years of continuous data. The seismic deployment in the Aegean region of Turkey including Izmir has been improved since 2008, after the enhancement of the AFAD-IzmirNET small-aperture local array, a collaboration of the AFAD and DEU-Dokuz Eylul University (Polat *et al*., 2009; Gok and Polat, 2014). The IzmirNET network improved P and S wave travel times collected by other seismic stations operating with a nearly six-year recording time. We have also added the data from International Seismological Centre (ISC, 2003), around the study area. To improve the solution quality, different earthquake catalogues recorded by different types of instruments were merged. The stations were equipped with three-component instruments such as Guralp CMG-3T, Guralp CMG-3ESP, GeoSIG GMS-Plus, and Guralp CMG-5TD.

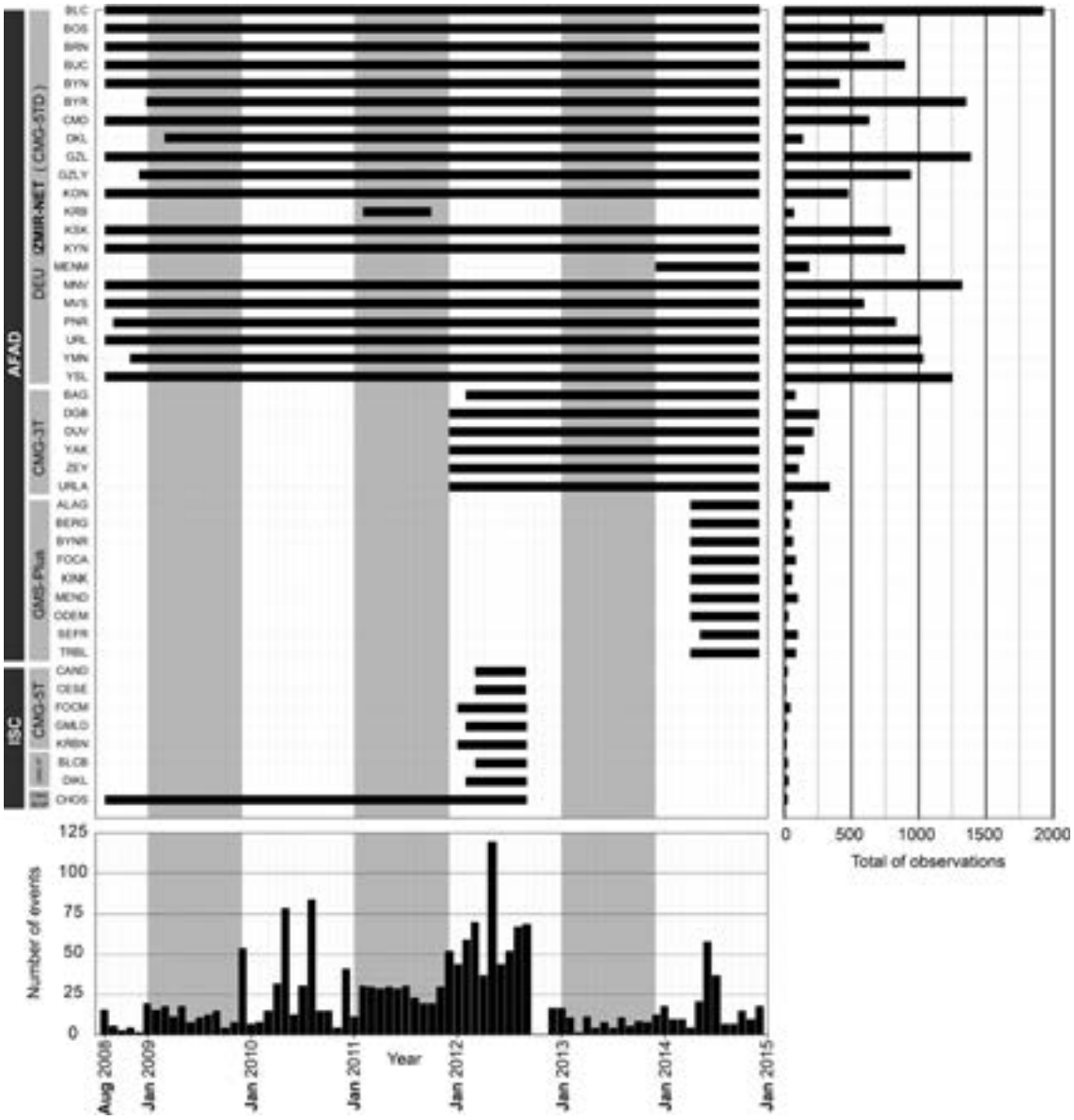

Fig. 2 - Time sequence for operational period of earthquake stations and networks between August 2008 and December 2014. Operational time interval of most stations is longer than three years except some 5T and GMS-Plus stations. The right histogram shows the total phase readings by each station. Bottom graphic presents total number of recorded events per month. Dense earthquake concentration is observable between 2011 and 2013. Abbreviations; AFAD: Earthquake Department of the Disaster and Emergency Management Presidency in Ankara-Turkey, ISC: International Seismological Centre.

During the data acquisition, we collected 15,924 P and 13,188 S picks from 1757 earthquakes with a magnitude equal to, or greater than, 2.0. Picks also include phase travel times from stations located outside the study area (Fig. 3). Most of the stations were concentrated in a rectangular area located between 26.20-27.75°E longitudes and 38.00-38.80°N latitudes. Sparse seismic clusters are evident as a result of the active extensional and compressional tectonics. Swarms are observable to the south and east of DH, around the SB area, along with the NW-SE direction in the Outer Bay and south of the eastern extremity of the Gulf of Izmir.

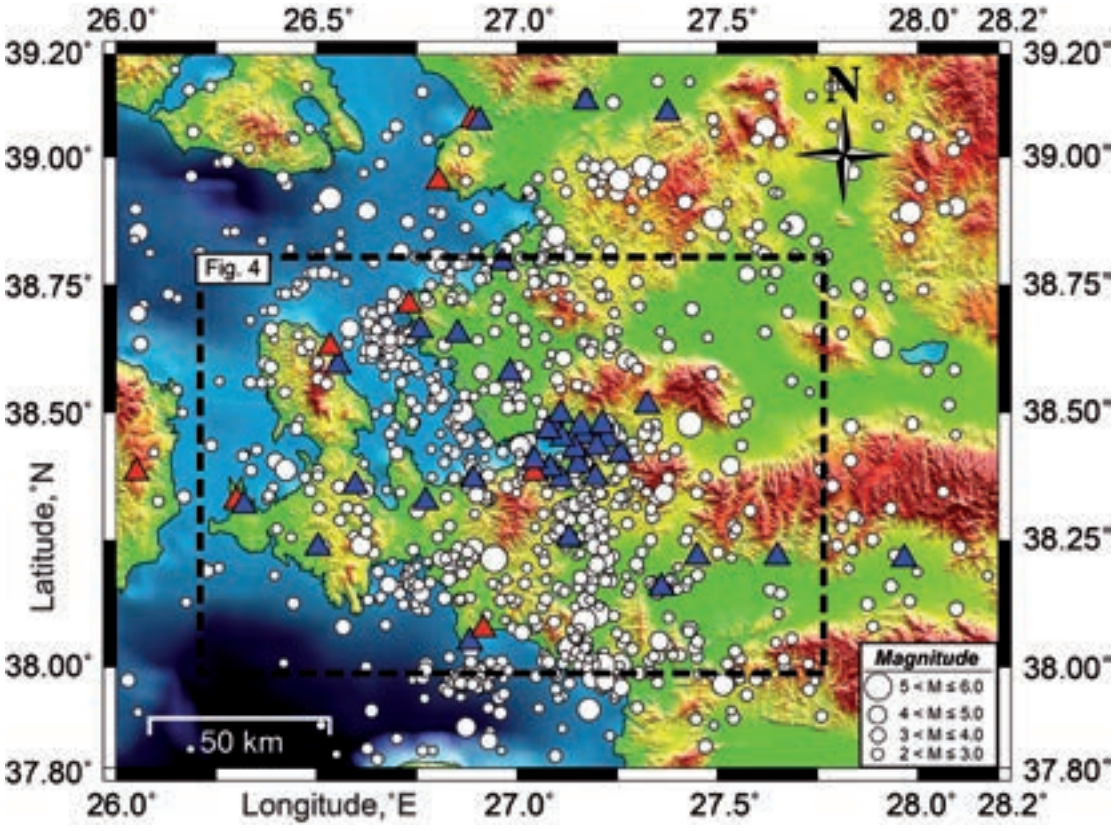

Fig. 3 - Seismic activity of the study area during the period from August 2008 to December 2014 showing 1757 events in total ($M \geq 2.0$). Filled triangles indicate 44 seismic stations. White circles show location of earthquakes. Dashed rectangle displays the focused area in the present study. Blue triangles show the IzmirNET local station array deployed by the DEU and AFAD (hand-picked). The red triangles show other instruments (ISC) used in the study. Events display clear swarm activity around the Outer Gulf of Izmir and Sigacik Bay. We also detected a NE-SW aligned cluster on Orhanli Fault Zone.

We have established two principal criteria to select the data. First, the total number of P and S readings for each event should be at least 11. Secondly, their 1D residuals (average 1D RMS residual value: 0.11 s) must be smaller than that of the initial model for P and S waves of 0.3 and 0.5 s, respectively. Selection of S-wave arrivals often creates difficulty in obtaining accurate locations and that results in reliable velocity models with higher resolution. However, the high level of background noise in seismograms and the weak amplitudes of P-wave arrivals may cause inaccurate selection, whereas S waves are much clearer in the Izmir case (Kececioglu *et al*., 2012). The 1D seismic velocity model (Ozer and Polat, 2017) and locations of 783 local earthquakes recorded by 44 stations were obtained after several attempts (Table 1).

In order to predict the effect of noise on resolution besides the optimal values of inversion parameters, we applied some synthetic tests as reported in Totaro *et al*. (2014). This synthetic travel time data were calculated for the source-receiver pairs as in the case of observed data. The locations of real earthquakes correspond to the solution provided after seven iterations of real data inversion. The synthetic data were perturbed with random noise having the average deviations of 0.2 and 0.4 for the P and S data in this study, reducing some values of variance as in the case of real data inversion.

Table 1 - The starting 1D reference model for P velocity (Ozer and Polat, 2017).

Depth (km)	P- wave velocity (km/s)
-2.0	3.1
2.0	4.2
10.0	4.7
12.0	6.2
18.0	6.5
25.0	7.5
30.0	7.7
50.0	8.5

3.2. Inversion procedure

The local tomography software (LOTOS) developed by Koulakov (2009) is used in the present study. It simultaneously inverts both P- and S-velocity distributions, hypocentral corrections (four parameters for each source), and station corrections. The latest parameter is important, because our data set includes some stations located outside the study area. Station corrections help to reduce the effects on travel time between the boundary of the study area and the station. Station coordinates and P and S arrival times are needed as input, without any *a priori* information on the earthquakes' location or origin time. The search for the earthquake location starts from the centre of the network or the station with minimal travel time. The inversion procedure includes the iteration of location and inversion steps. It first simultaneously optimizes the best 1D velocity model and locates preliminary hypocentres. For this step, it uses a grid-search method and tabulated travel times that were previously computed for a 1D velocity model. In the vertical direction, the grid spacing depends on the data density, but it cannot be smaller than a predefined value. A bending algorithm is, then, used to perform ray tracing to move the sources in a 3D velocity model. This algorithm is fast and performs reliable computations of travel times between two locations. The next step calculates the parametrization for the first iteration (Jaxybulatov *et al.*, 2011). It regularizes the solution by minimizing the gradient. The grids are based on vertical lines distributed regularly in a map view (in this study with steps of 5×5 km). To avoid any bias related to the basic orientation of the grid, we performed the inversions for several grids with different basic orientations (0°, 22°, 45°, and 67° in our case). The LOTOS algorithm uses a matrix calculation and includes the elements responsible for station and source corrections (four elements for each source). The sparse linear equations and sparse least squares (LSQR) method (Paige and Saunders, 1982; Nolet, 1990) inverts the large sparse matrix. In the final stage, the inversion is damped by adding special regularization matrix blocks for amplitude tuning and smoothing. After computing the inversion in differently oriented parameterization grids, a mean model is calculated in a regular grid, and it is used as a starting 3D velocity distribution for the subsequent iterations. Synthetic modelling is used to estimate a few variables, such as grid spacing, smoothing coefficients, amplitude damping, weights, and the number of iterations, for the inversion at different depth levels. Minimum average deviations of residuals and maximum numbers of events are also obtained from the best model (Jaxybulatov *et al.*, 2011; Totaro *et al.*, 2014).

We run seven iterations and compute the reduced values of ~23% and ~26% for P- and S-wave arrivals. The RMS perturbations are 0.13 and 0.19 s (Table 2). The best result for the LET study identified 783 selected events with 7676 P and 6431 S readings, showing 18 picks for each event (Fig. 4). However, many events are detected beneath the Quaternary and Neogene basin located between SH and NM (towards the south of the IzmirNET array).

Table 2 - RMS values of the P- and S-wave travel time residuals and the variance reductions for V_p and V_s.

Iteration	rms P (s)	rms S (s)	reduction P (%)	reduction S (%)
1	0.1720	0.2514	0	0
2	0.1510	0.2169	11.6871	13.7177
3	0.1416	0.2012	17.1739	19.9878
4	0.1373	0.1936	19.7129	22.9886
5	0.1356	0.1891	20.6834	24.7840
6	0.1346	0.1873	22.4710	25.8690
7	0.1327	0.1865	22.5677	25.9009

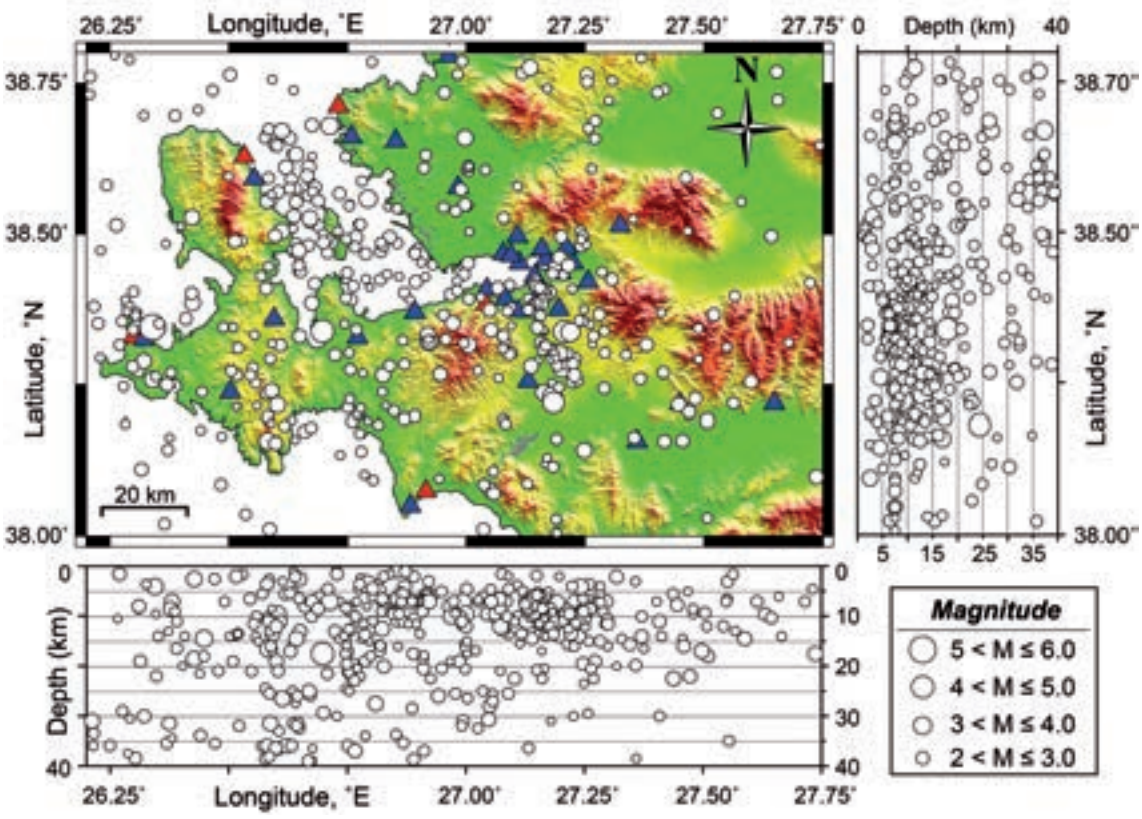

Fig. 4 - Vertical depth cross-sections of 783 selected events along the E-W and N-S directions. White circles symbolize final locations. It is clearly observable that earthquakes are generally located in the first 30 km of Earth crust.

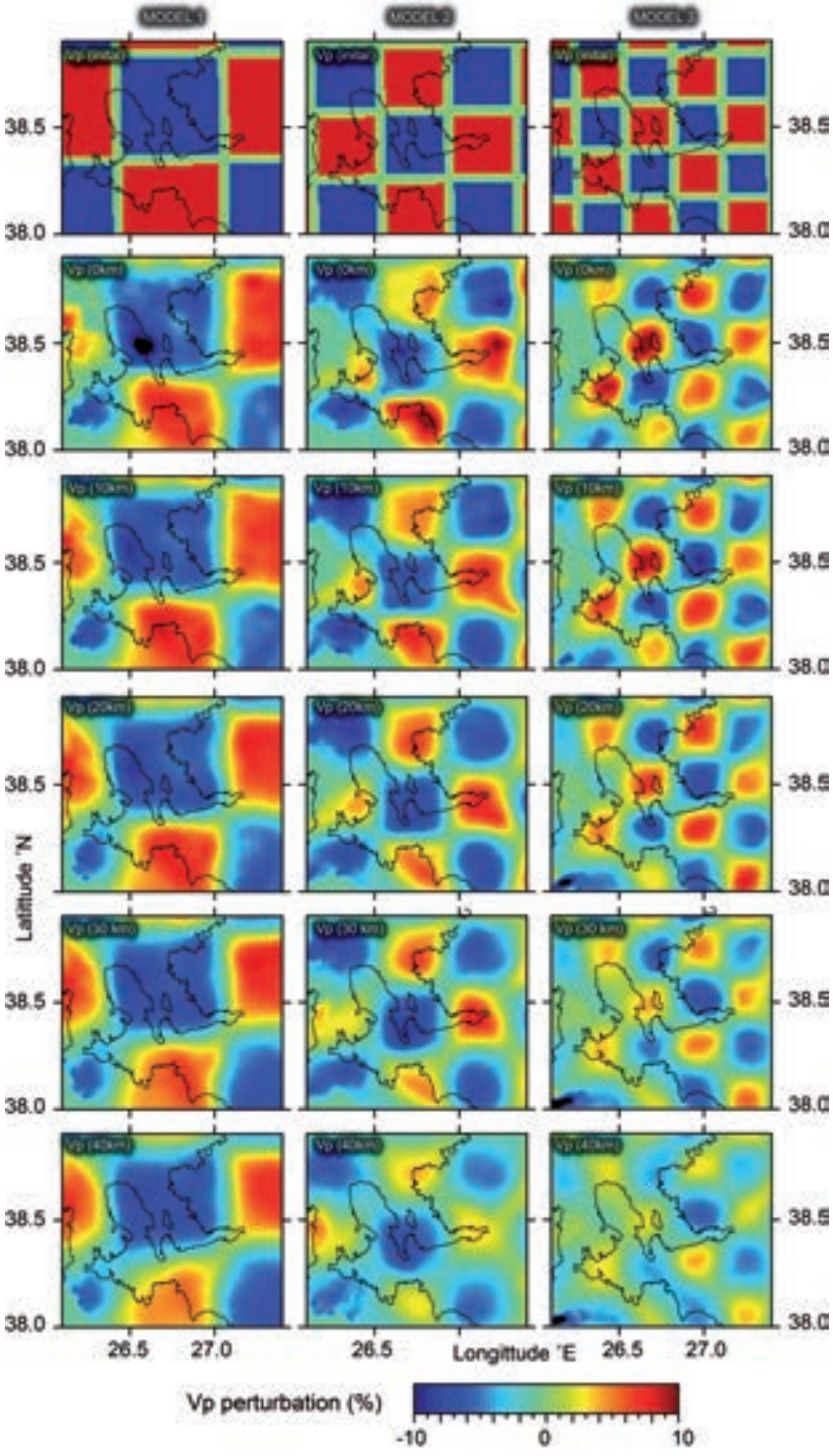

Fig. 5 - Periodic positive (red color) and negative (blue color) P anomalies show 10% velocity perturbations in different block sizes: 50 km for Model 1, 30 km for Model 2, 20 km for Model 3, with 5 km empty spacing (top of the figure). Checkerboard tests, conducted to evaluate the spatial resolution and estimate the optimal values of inversion parameters, have been defined for 0, 10, 20, 30, 40 km depth levels. Solid lines represent coastlines of the study area. The anomalies are well reconstructed down to 30 km depths, but resolution is poor at levels deeper than 30 km due to the lack of events.

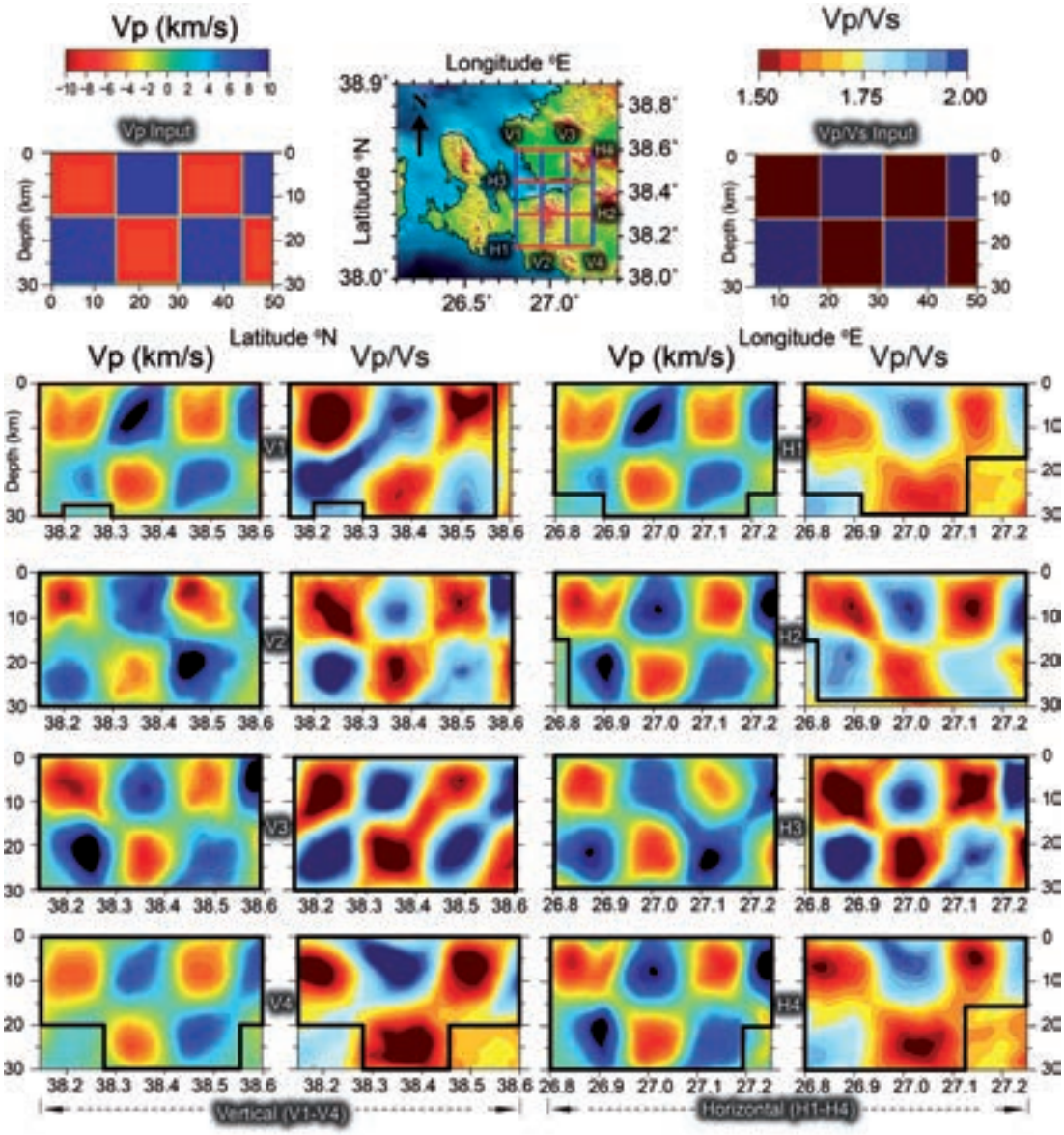

Fig. 6 - Benchmark for testing the vertical resolution using the checkerboard model. Anomalies change ±10% for P-wave velocities. *Vp*/*Vs* ratio ranges from 1.5 to 2.0. The input model with block size of 15×15 km^2 is conducted to evaluate the reliability of vertical depth cross-sections. Outcomes in different profiles are satisfied to understand velocity structure of Earth crust. Well-resolved areas (shown as thick lines) show that tomograms can be interpreted with confidence.

3.3. Resolution test

We estimate the optimal velocity values of inversion parameters and spatial resolution by using checkerboard tests. We present three different checkerboard tests. In these tests we described periodic negative and positive velocity anomalies (5 km/s) of their different dimensions: 50 km for Model 1, 30 km for Model 2, 20 km for Model 3, and 5 km empty intervals for each model (Fig. 5). We have performed several synthetic tests to resolve the noise effect and optimum values of inversion. For the same source-receiver pairs, we computed synthetic travel times as in the

case of the observed data. At the seventh iteration, the locations of real sources were obtained in corresponding real data inversion. We then followed a similar process for real data analysis, introducing the absolute source location. It can be seen that spatial models for V_p almost for all depth sections are reconstructed in central parts of the study area with the anomaly sizes of 10 km showing a distinct separation between the Gulf of Izmir and Sigacik Bay areas. However, the resolution decreases in the eastern and western extremities of the study area, as clearly seen in the layers at 30 and 40 km of depth, due to the lack of data (Fig. 5). On the other hand, we conducted the vertical checkerboard test to show the stability of vertical models; the input model used to compute it has velocity anomalies changing W-E direction at ±10% and from 1.5 to 2.0 for V_p and V_p/V_s, respectively. The vertical resolution is considered to be good down to 30 km for areas where the vertical checkerboard image is reconstructed. According to the vertical checkerboard test outcomes, the capacity of data and station coverage can resolve the Izmir region and its near surroundings to between 0 and 30 km. The resolution reduces at 25 km of depth and below owing to the low ray density (Fig. 6). Regarding these trials, it is possible to estimate the patterns for different parts of the study area. Additionally, these tests show that the inversion parameters are identical for real and synthetic data inversions, and they can be evaluated as adequate to provide optimal solutions.

4. Results

Izmir and its surroundings present significant hydrothermal activities that can be easily triggered/developed by fragmented ruptures and reveal a high potential for geothermal resources. Different fault systems distributed all along the Izmir area control the evolution of the geothermal activity. We report below new V_p, V_s, and V_p/V_s anomalies in both horizontal and vertical cross-sections from local earthquake tomography inversion for the Izmir geothermal region.

4.1. Horizontal depth slices

Horizontal cross-sections are constructed at depths of 2, 10, 15, 20, 25, and 30 km, where a sufficient ray path coverage is provided. In all sections, prominent low and high V_p and V_s anomalies can be seen for different depths down to 30 km. The maximum and minimum perturbations between the initial and final velocity models vary approximately ±10%. Findings from different layers reveal that velocity models show significant low-velocity anomalies down to the lower crust, deeper than expected. The V_p/V_s ratio ranges from 1.5 to 2.0. Plane views are presented in Fig. 7 showing V_p and V_s perturbation within well-resolved areas.

In general, low velocities in the shallow layers can be ascribed to severe fracturing, fluid-filled formation in rock matrix and weak materials (Serrano *et al.*, 2002). Low velocities are also the expression of thermal conductivity, presence of high heal flow, and attenuated fragments consistent with the influx of asthenosphere to shallow depths as a result of ongoing lithospheric extension (Dolmaz *et al.*, 2005; Salk *et al.*, 2005; Tarcan *et al.*, 2009; Delph *et al.*, 2015).

4.1.1. Slice at 2 km

Negative V_p perturbations of up to -8% are evident at the western end of Inner Bay in the Gulf of Izmir (NW area of the BGS), in the UI along the E-W direction, and for a large area beneath

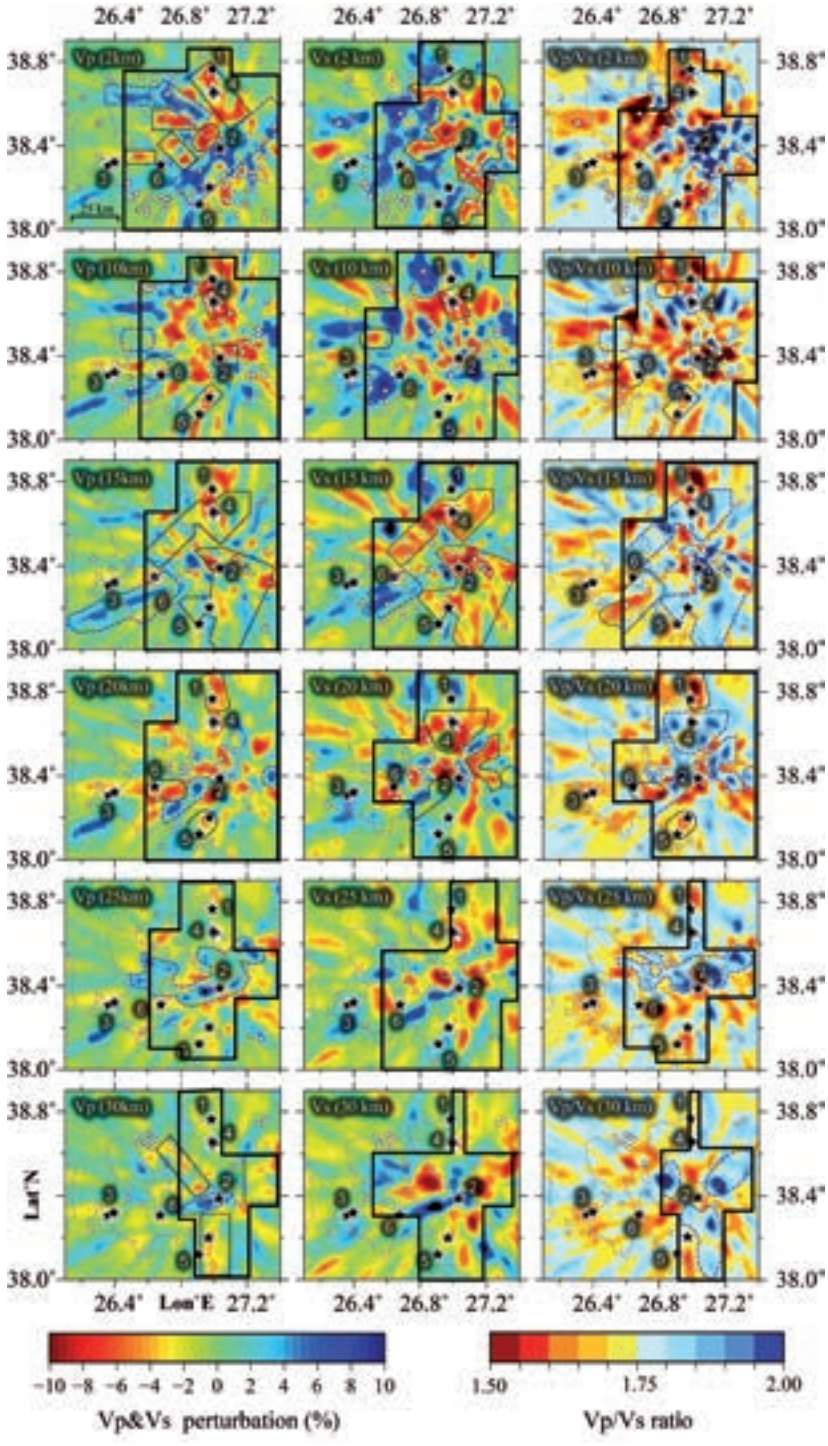

Fig. 7 - Spatial variation of V_p, V_s, and V_p/V_s models for depths 2, 10, 15, 20, 25, and 30 km. Velocity images and V_p/V_s models are indicated by the perturbations in percent (±10%) and the ratio (ranging from 1.5 to 2.0), respectively. Stars represent geothermal areas, and white circles show earthquake hypocentres that are projected onto slices with ±2 km depth differences (focal depth of earthquakes between 0-4 km, 8-12 km, 13-17 km, 18-22 km, 23-27 km, 28-32 km for 2, 10, 15, 20, 25, 30 km depth slices). Dashed and dotted lines show locations of positive and negative anomalies, respectively, which are mentioned in the text under "Results". Main geothermal systems 1: Aliaga-AGS, 2: Balcova-BGS, 3: Cesme-CGS, 4: Menemen-MGS, 5: Seferihisar-SGS, 6: Urla-UHS.

MGS along a NW-SE direction. Smaller negative V_p anomalies are found between UHS and CGS, east of UHS aligned NW-SE (dotted lines at V_p of Fig. 7). Similar negative V_p changes were also observed near the CGS, even if the resolution is low. Geological contacts and rupture zones also reveal the low V_p (together with low V_s) anomalies. The 2 km slice within our tomographic model is related to distributions of the Quaternary alluvial units. In contrast, positive V_p anomalies of about +8% extend from 26.8°E (Seferihisar High) up to 27.3°E along a NE-SW direction in the BGS (dashed lines at V_p of Fig. 6). Other remarkable positive V_p anomalies are located close to the offshore area of the Outer Bay (aligned NW-SE) and north of the KP. The distribution of large scale S-wave velocity negative anomalies down to -8% (dotted lines at V_s of Fig. 6) is visible close to the eastern half of the resolved area. Low velocity ratios down to 1.6 (dotted lines at V_p/V_s of Fig. 6), together with low V_p velocities in the shallow layers, are likely the outcome of high fluid saturation and poorly consolidated material. It is evident that decreasing S-wave velocities results in a high V_p/V_s ratio which is interpreted as saturated and highly fractured formations that comprise high fluid pressured volumes. Deposits around Inner Bay of the Gulf of Izmir are characterized by low V_p (with low V_s) and high V_p/V_s, possibly reflecting water-saturated sediments at shallow depths (see dotted lines at V_p, V_s, and V_p/V_s in Fig. 7).

4.1.2. Slice at 10 km

Contrary to the upper slice, at 10 km, low V_p/V_s ratio (except near MGS) and V_p (with normal to positive V_s) anomalies are found near the geothermal areas (dotted lines in Fig. 7). Their position is consistent with tectonic features and edges of the graben systems surrounded by the Quaternary and Holocene alluvial units. A sharp transition of the V_p/V_s ratio (from high to low) is observed around the eastern extremity of the Gulf of Izmir (dashed lines at V_p/V_s of Fig. 7). It is reported that sedimentary deposits formed by the graben systems show this type of velocity perturbation along the coastal areas (Tarcan *et al*., 2005; Serpen *et al*., 2009; Magri *et al*., 2012). High-to-normal V_p/V_s and negative V_p (with negative V_s) anomalies are evident near the MGS area (see dashed and dotted lines, respectively, in Fig. 7). This variation can be interpreted as a result of hydrothermal activity. Regardless of whether this type of perturbation is reported at shallower layers, we observed these anomalies at an approximately 10 km depth layer. In contrast to these assignations, a clear positive V_p and V_s anomalies (with low V_p/V_s) is also evident to the NW of the MGS (dashed lines in Fig. 7). These bodies may mainly represent deep roots of Neogene-aged basaltic, andesitic, and rhyolitic volcanic. Similar to the MGS, positive V_p (>4.0%) and V_s velocities with normal-to-high V_p/V_s ratio are observable in the KP. This area is located beneath mountain regions towards the SW of the UHS (dashed and dotted lines, respectively, in Fig. 7). This result shows a general agreement with the main geological features of the KP, which are formed by Miocene-aged volcanics and Palaeozoic-Mesozoic-aged basalts (Aldanmaz *et al*., 2000; Ersoy *et al*., 2014).

4.1.3. Slice at 15 km

The compaction of geological features at depth may increase the pore pressure. Large-scale negative perturbations can be recognized from V_p and V_s anomalies (dotted lines in Fig. 7). The V_p/V_s ratios increase from 1.8 to 2.0 within the same area (dashed lines in Fig. 7). These high V_p/V_s together with low V_s perturbations are evident beneath mountain areas such as Nif, Spil, YM and Seferihisar High. This anomaly combination can be interpreted as the existence of porous

and highly water-saturated fractured zones (Cevikbilen *et al*., 2012; Kaypak and Gokkaya, 2012; Khrepy *et al*., 2015). If the V_p distribution is compared with the distribution at a 10 km depth slice, we observe a sharp decrease in negative V_p anomalies. Normal-to-positive V_p and V_s bodies (dashed lines at V_p and V_s of Fig. 7) with a low V_p/V_s ratio (dotted lines in Fig. 7) tend along the NE-SW direction by reaching up to +10% to the SW of UHS. The outcrop of volcanic rocks, granites, and magmatic materials situated at the deeper parts as members of the Menderes metamorphic massif, are responsible for higher-velocity anomalies.

4.1.4. Slice at 20 km

The V_p pattern at 20 km shows dispersed negative velocity zones (-8%). These structures also have a low V_p/V_s ratio near UHS, AGS, and SGS (dotted lines at V_p, V_p/V_s of Fig. 7). We notice positive V_p (with negative-to-normal V_s, high V_p/V_s) perturbations (+8%) to the SE of UHS along a NE-SW direction and the Spil Mountain at 27.3°E longitude (dashed lines at V_p, V_p/V_s and dotted lines at V_s of Fig. 7). In general, high V_p/V_s anomalies (>1.95) are mainly dispersed to the east of the study region starting from 26.8°E, with negative V_s in the same area. This distinguishable separation may represent a variation in the depth range from the thinner to the thicker crust beneath the research area as reported for some cases in different studies (Gessner *et al*., 2013). We interpret these lateral variations as a slight increase in the crust towards the east of the study area.

4.1.5. Slice at 25 km

Most areas located beneath the geothermal systems exhibit normal V_p and normal-to-high V_p/V_s anomalies. However, negative V_p and V_s patterns radically decrease by exhibiting dispersive distribution. Positive V_p anomalies (+9%) are observable at the centre of the research area including the BGS (dashed line of Fig. 7). The southern coastline of the Gulf of Izmir following the IFZ reveals positive V_p changes (+6%) along an E-W direction. The same observation (high values) can also be followed for the V_p/V_s ratio, indicating partial thermal melting of the subcontinental lithospheric mantle with different degrees of silica saturation (Ersoy *et al*., 2010; Gessner *et al*., 2013).

4.1.6. Slice at 30 km

Seismic velocities are characterized, as in the above slice, by a lower spatial resolution. Negative V_p anomalies are less pronounced (-4%) in comparison with shallower slices and are found along the NW-SE coast of Outer Bay, south and east of the study area (dotted lines in Fig. 7). Velocity perturbation for the positive V_p band (+4%) shows a remarkable decrease along the southern coastline of Inner Izmir Bay compared with the previous layer (dashed lines in Fig. 7). The V_p/V_s ratio increases (>1.9) towards the eastern part of the study area (dashed line in Fig. 7), representing variable degrees of melting of the metasomatized mantle assembled with garnet-amphibole, and subsequent differentiation processes such as magma mixing, assimilation, and fractional crystallization (Ersoy *et al*., 2008; Helvaci *et al*., 2009).

4.2. Vertical depth cross-sections

To better constrain the crustal velocity structure of the Izmir geothermal area, we have generated vertical depth cross-sections of the V_p and V_p/V_s models previously unavailable for the study area (Fig. 8). Highly resolved seismic patterns have been shown along the vertical sections as parallel

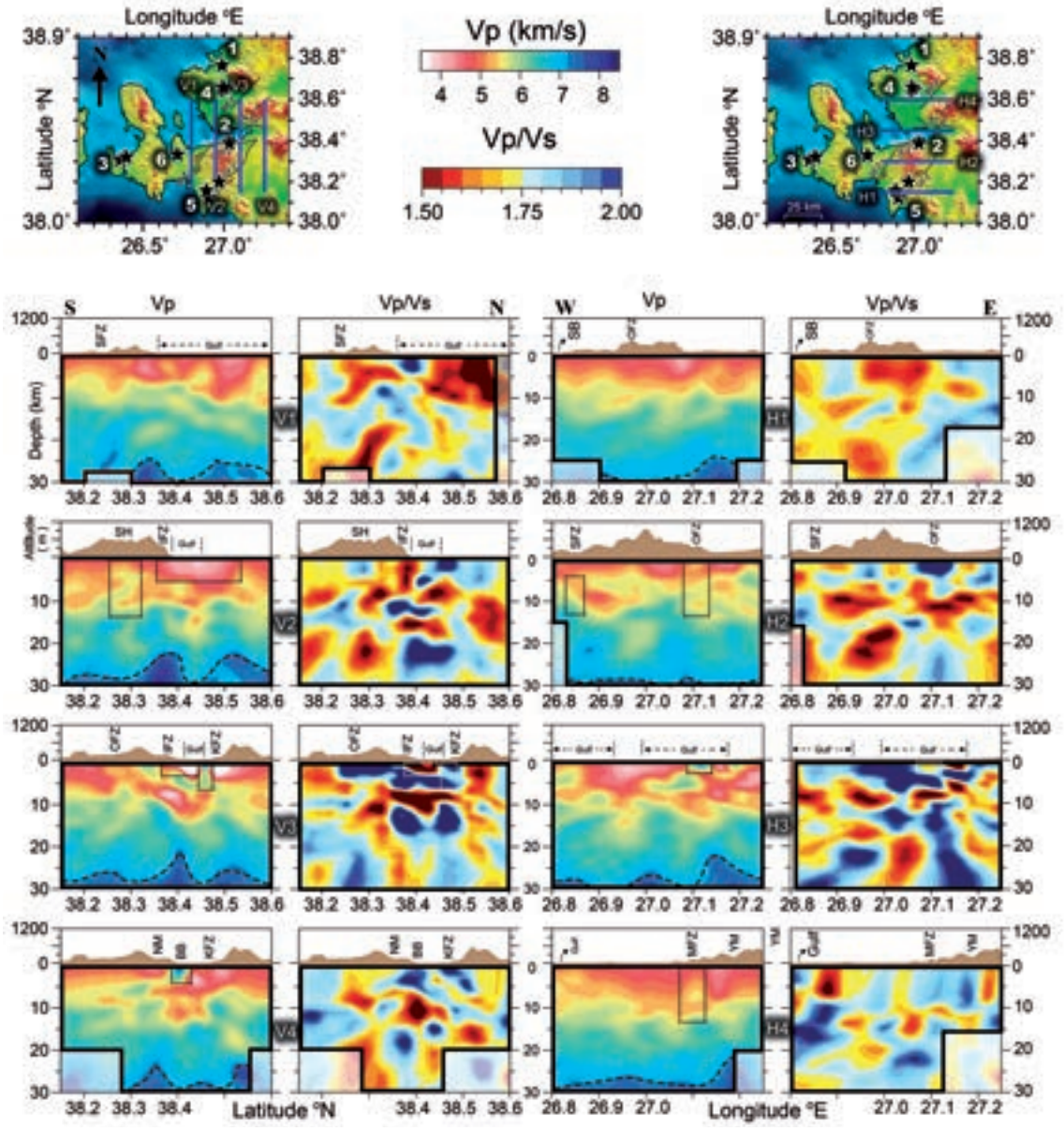

Fig. 8 - Location of traces for depth cross-sections that are oriented along the N-S (between V1 and V4) and E-W (from H1 to H4) directions in the study area. Absolute P-wave velocities (ranging 3.5-8.5 km/s) and V_p/V_s ratio (between 1.5 and 2.0) tomographic models obtained from this study reveal seismic features down to 30 km of depth. Mantle boundaries are shown as dashed lines. Dotted lines show the locations of velocity anomalies mentioned in the text under "Results". Blurred images indicate less reliable areas due to lack of ray paths. NM: Nif Mountain, SH: Seferihisar High. Main geothermal systems 1: Aliaga-AGS, 2: Balcova-BGS, 3: Cesme-CGS, 4: Menemen-MGS, 5: Seferihisar-SGS, 6: Urla-UHS.

and perpendicular profiles to each other. Regardless of whether calculations were performed for much deeper and larger areas, velocity anomalies at the vertical section are only resolved down to a 30 km depth owing to what data was available.

The lowest V_p values are observed in the basin located towards the east of the Gulf of Izmir (3.5-4.0 km/s) down to a 4 km depth. High V_p values at anomalously shallow depths in some

profiles (e.g., V3, V4, H3) might be explained in different ways. The lowest V_p/V_s ratio (~1.5) has been detected as a ~10 km spatial length down to 2 km beneath the northern end of Seferihisar High (e.g., V3). The largest V_p/V_s values (1.75-1.95) were observed beneath Seferihisar High (e.g., V2, V3) down to a 25 km depth and around the OFZ (e.g., V3, H2). The V_p/V_s ratio increases (~1.9) towards the eastern end of the Gulf of Izmir (e.g., V3, H3).

The 3-D vertical velocity models consist of four main layers. In general, we have identified four main crustal layers ranging in depth from the surface to 30 km.

4.2.1. Upper crust (0-7 km)

The mean uppermost layer of the low V_p model lies at ~5-7 km beneath the IFZ, basin structures, and the Gulf of Izmir from small- to large-scale spatial lengths (e.g., V2, V3). Reflecting the near-surface geology such as Neogene sediments and Quaternary alluvial deposits, results in this V_p change at the top layer. The calculated low V_p velocities range from 3.5 to 4.8 km/s, particularly by extending beneath the IFZ down to 3 km depths (e.g., V3). The low V_p patterns beneath the KFW seem to be mutually inclined towards each other (e.g., V3). The deepest edges of the basin formed by the KFZ represent high V_p (>6.5 km/s) and high V_p/V_s (1.75) anomalies which are consistent with the topographic slopes located at the north of the gulf beneath the KFZ (e.g., V3). Because there is a close link between irregular basement shapes (e.g., Bornova Basin) and velocity anomalies near geothermal areas, the presence of the fluids along the fault zones may explain the high V_p/V_s anomalies (e.g., V4, Khrepy *et al.*, 2015). This appears to be consistent with the orientation of normal faults identified in this area from geologic observations (Uzel *et al.*, 2012). The high V_p bodies extend up to anomalously shallow depths as observable in V3, V4, and H3 profiles. The thickness of the first (low-velocity) layer (0-7 km) dramatically decreases beneath the Seferihisar High with increasing V_p values (e.g., V2). We detect gradually high V_p (~5.2 km/s) beneath the SFZ, OFZ, and MFZ (e.g., V1, V3, H2, H4) drifting up to shallow layers.

4.2.2. Middle crust (7-15 km)

The V_p model provides some information about the internal properties of the different geological units between 7 and 15 km depth layers. The most significant V_p features of this layer (middle crust) are the presence of a thickening tendency towards the north and east slightly visible at depth cross-sections (e.g., V1-V4 and H1-H4 except H2). High velocities are observable beneath the Seferihisar High (e.g., V2), SFZ, OFZ, and MFZ (e.g., V1, V3, H2, H4) ranging from 5.0 to 6.0 km/s, approximately. These bodies may represent lithospheric crystalline rocks that intruded into the upper crust.

4.2.3. Lower crust (15-27 km)

Kaypak and Gokkaya (2012) identified a V_p velocity of approximately ~6.5 km/s between 10-20 km for the Denizli Basin (located to the eastern extremity of the Aegean region). We resolved this layer well with V_p velocities ranging from 6.2 to 7.2 km/s. This sharp increase in V_p velocities reveals the variation of the rock composition in the study area, where heterogeneous rock units such as the tectonic melanges of the Bornova Flysch zone may respond to the ductile flow of the lower crust (Gessner *et al.*, 2013). These velocities could also be explained by the presence of gabbro, increased process of serpentinization and other crystalline rocks (Hauksson, 2000).

4.2.4. Mantle (>27 km)

An acceptable resolution is found only in areas where the deepest earthquakes are present. Values of the resolution are low because of the existence of few recording stations and the low seismicity rate. Deeper velocities are related to some intrusive bodies towards the lower crust beneath the southern Gulf of Izmir (V1, H3), IFZ (V2, V3), Nif Mountain (V4), OFZ and SFZ (H2), and Yamanlar Mountain (H4). From the data, we estimate the crust/mantle transition at a ~27 km depth with high V_p rates (≥7.5 km/s) as an undulated boundary, which is in agreement with other geophysical studies (e.g., Salah *et al*., 2007; Komut *et al*., 2012; Salaun *et al*., 2012; Karabulut *et al*., 2013; Tezel *et al*., 2013) and represents a global average on the lower bound of P-wave velocities (Ustaszewski *et al*., 2012). A similarly fluctuating shape of the Moho boundary is also observed in the Erzincan and Denizli cases (Kaypak, 2008; Kaypak and Gokkaya, 2012; Karabulut *et al*., 2013). The resolution gradually decreases with increasing depth, with the V_p model still showing, however, an acceptable level of resolution in the depth range of 0-27 km beneath the study area.

5. Discussions

Studies of thermal fluids, heat flow measurements, and reported temperatures are well above normal values in Izmir and its surroundings (Yilmazer and Alacali, 2005; Erkan, 2015) as also confirmed by using Curie-point depths (Aydin *et al*., 2005; Aksoy *et al*., 2008). Other geophysical measurements such as microgravity and magnetic study models (Ates *et al*., 1999; Duzgit *et al*., 2006; Pamukcu and Yurdakul, 2008) performed along grabens and mountainous areas, are in line with the present velocity anomalies obtained in the frame of this study. It is evident that new findings that exhibit low V_p (<4.6 km/s) and low-to-normal V_p/V_s (<1.7) ratio could be associated with a high gas/fluid content of the material in the region by indicating new possible geothermal areas.

To improve the interpretation for Aliaga (AGS), Balcova (BGS), Menemen (MGS), Seferihisar (SGS) geothermal systems, and Urla hot springs (UHS), we have decided to project the region using two perpendicular profiles along N-S (Profile A) and E-W (Profile B) directions (Fig. 9). Interpretations for the Cesme (CGS) geothermal system may not be fully meaningful regardless of whether it is located just at the boundary or outside the resolved area.

5.1. Aliaga geothermal systems (AGS)

A low V_p (<4.4 km/s) and low V_p/V_s (<1.60) ratio are clearly seen beneath the AGS (1) down to 8 km depth layers (Fig. 9, profile-A). The mean temperature of the hot fluid is approximately 98°C at the surface. Hotter crust and higher heat flows can characterize these zones as also discussed by Lees and Wu (1999), Sherburn *et al*. (2003) and Aydan *et al*. (2005). Two new geothermal resources were discovered in 2015 in Samurlu belonging to the AGS with a temperature of 90°C. In 2016, one of them already started to contribute to the geothermal power generation capacity of Turkey, which has increased from 30 MW in 2008 to currently 648 MW as of May 2016 (Ozer and Polat, 2016a, 2016b). We believe that the AGS area still presents desirable targets for more new geothermal potentials if dense site-specific studies are performed with seismologic sensors by using active/blast sources.

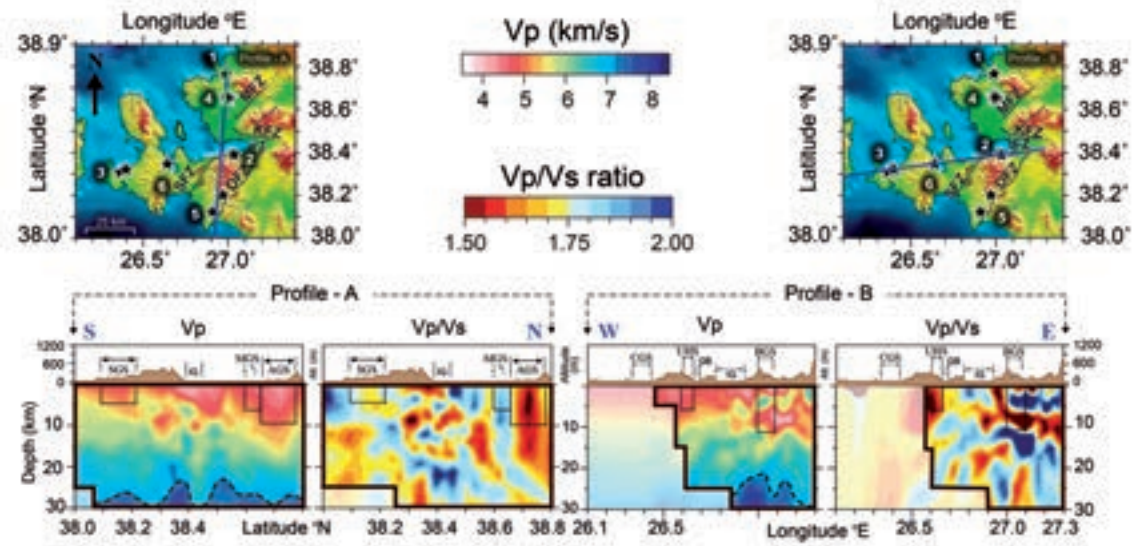

Fig. 9 - Depth cross-sections of the V_p and V_p/V_s anomalies crossing the Izmir geothermal area along the N-S (Profile A) and E-W (Profile B) directions. Four different layers have been identified with distinct colour changes down to Moho (shown as dashed lines at about 27 km depths). Dotted lines show the locations beneath geothermal systems mentioned in the text under discussion caption. Main geothermal systems 1: Aliaga-AGS, 2: Balcova-BGS, 3: Cesme-CGS, 4: Menemen-MGS, 5: Seferihisar-SGS, 6: Urla-UHS.

5.2. Balcova geothermal systems (BGS)

Similar to the AGS, low V_p (<4.3 km/s) and low V_p/V_s (≤1.75) anomalies close to the surface are evident beneath the BGS (2) (Fig. 9, Profile B). The reported temperature here is approximately 140°C. However, the BGS differs in its signature from the AGS. BGS shows negative Bouguer gravity anomalies as discussed in detail by Akgun *et al*. (2014) and Pamukcu *et al*. (2014, 2015b). Low V_p, low V_p/V_s anomalies are found at two different depth layers of 0-2 km and 5-11 km. Geothermal facilities are mostly generated by the fluids located at shallow depths. However, we report that a 2-5 km layer (low V_p, high V_p/V_s) must also be evaluated as a new possible geothermal resource not yet drilled. A normal-to-high V_p (>6.3 km/s) and high V_p/V_s (>1.95) layer is also detectable between 2-5 km depth. This high V_p, high V_p/V_s anomaly can be linked with water-saturated cracks (low V_s) or high pore fluid pressures. Deeper depths of the BGS (11-30 km) exhibit transitions between high (>1.95) and low (≤1.7) V_p/V_s perturbations. As we can conclude from the events located at deeper depths (Fig. 4), these transitions are reasonably resolved based on our data set.

5.3. Menemen geothermal systems (MGS)

It is located to the south of the AGS and reveals a similar low V_p (<4.5 km/s) body down to 6 km. However, its velocity ratio is quite different from the AGS, revealing high V_p/V_s of >1.75 (Fig. 9, Profile A). This area is located at the boundary of volcanics and sediments. Neogene Foca volcanics overlie alluvial-fan and lower-sedimentary units. This composition increases the pore pressure, resulting in observations of high V_p/V_s. Low V_p, high V_p/V_s structures are mainly located at the shallow depths beneath MGS (4 in Fig. 10), indicating high fluid/melt contents by the high flow-rate. As an important thermal body of Izmir, the region can be evaluated as a possible magma intrusion, considering its high Curie temperatures (560-580°C) and heat flow rates (120

mW/m^2) marked as maximal in the study area (Dolmaz *et al*., 2005; Hosny *et al*., 2009; Shater, 2012). A low V_p and high V_p/V_s combination is reported for the shallow-to-middle crust as a result of decreasing S-wave velocities or reflecting water-saturated sediments (Hauksson, 2000; Kaypak and Gokkaya, 2012). The main water temperature of MGS is reported to be more than 55°C, but this field is known as one of the newest geothermal resources of Izmir (Ozkan *et al*., 2011) as the AGS, and still requires further specific studies.

5.4. Seferihisar geothermal systems (SGS)

Several hot springs occur in the central part of the SFZ and imply that the fault zone provides effective conduits for the SGS (5 in Fig. 10). It shows a clear low V_p (<4.6 km/s) and low-to-normal V_p/V_s (≤1.75) anomalies down to 4 km. Reported fluid temperatures at the surface change between 56° and 95°C. It seems possible that the presence of granitic outcrops in the Bornova Flysch zone (Seferihisar High) is responsible for the high V_p/V_s ratio (Gessner *et al*., 2001). Furthermore, low V_p/V_s (with low V_p) anomalies are also detectable beneath the southern part of the IG (an area located close to the BGS). This finding reveals that the number of potential geothermal resources near the BGS might be much higher than expected.

5.5. Urla hot spring (UHS)

Similar to the AGS, BGS, and SGS, the UHS (6 in Fig. 10) also presents clear low V_p (<4.6 km/s), low V_p/V_s (≤1.70) anomalies down to 6 km. However, the reported temperature is gradually much lower, registering 19-32°C at the surface. Geophysical measurements near the UHS indicate low self-potential, low resistivity, and high conductivity anomalies performed in the last decade (Drahor and Berge, 2006; Gurer and Bayrak, 2007; Sindirgi *et al*., 2008; Kaftan *et al*., 2011, 2014). As a part of western Anatolia where many geothermal resources are concentrated, the UHS area also needs a further seismological tomography survey to describe the GFZ, which is an important fracture zone, and to improve the resolution.

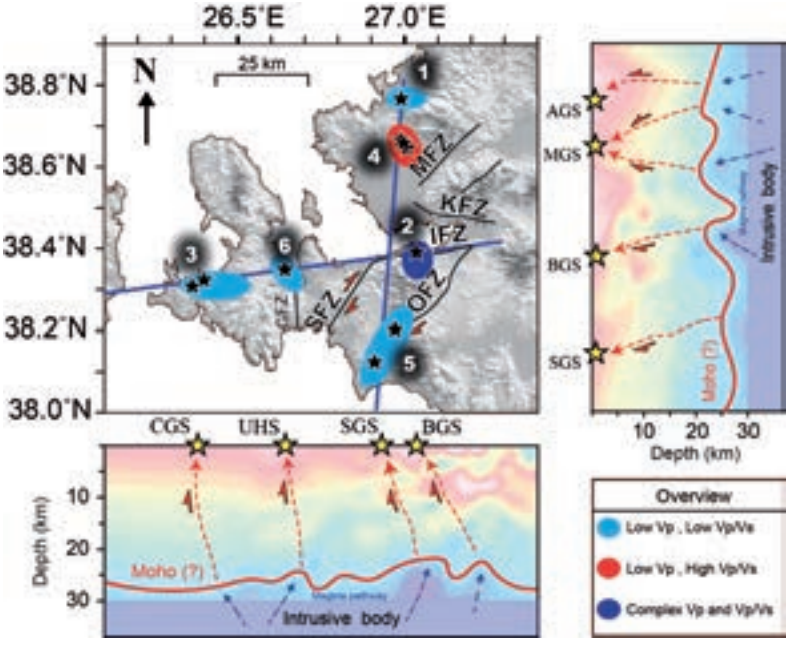

Fig. 10 - Interpretation cartoon for geothermal system beneath Izmir and surroundings. Moho depth is shown via red line. Stars represent main geothermal system. The background anomalies are the distribution of V_p velocities along profiles A and B, same as in Fig. 9. Red arrows depict the pathway of intrusive magma bodies. Blue arrows are shown the pathway of intrusive body. Main geothermal systems 1: Aliaga-AGS, 2: Balcova-BGS, 3: Cesme-CGS, 4: Menemen-MGS, 5: Seferihisar-SGS, 6: Urla-UHS. Based on the tomographic results, we can conclude that Menemen area (4) could contain geothermal fluid and Aliaga (1), Seferihisar (5), Urla (6) region may comprise a high gas and CO_2 content.

Our tomography inversion brings a new feature, as illustrated by the simplified model in Fig. 10, and suggests low-velocity zones beneath the Izmir geothermal area as shown from E-W and N-S profiles. The weak lower crust, which is likely to represent a magmatic intrusive body, constitutes a thick viscous layer (between 15 and 27 km) that mechanically decouples the brittle-elastic middle crust (7-15 km). Hauksson (2000) attributed the high-velocity anomalies to intrusive mafic rocks derived from the cooled mantle magma between 7 and 15 km beneath basin-type areas, as we also observed in the seismic profiles. High-velocity anomalies beneath the study area are related to high-density remnants within cooled Neogene volcanics during the late Miocene and Pliocene (Gessner *et al*., 2013) at the upper crustal layer (0-7 km). Structurally, current magma activities continue to occur beneath the hydrothermal systems of Izmir and its surroundings. Although the estimated mantle boundary is located at a depth of 25-27 km, it tends to extend to shallow depths beneath the Gulf of Izmir. Similar to this observation, there is a huge low-velocity zone beneath the BGS starting at depths of 5-7 km and exhibiting a rectangular area of ~20×7 km^2 size. Its transport system is probably linked to the partial melting or upwelling of the upper mantle.

6. Conclusions

This research presents the LET study in the Izmir geothermal area and provides significant insights about potential reservoirs not yet drilled. Detailed V_p, V_s, and V_p/V_s structures also provide important information about the crustal structure of the study area. To provide a basis for the results of the tomography models, we used earthquake data that are mainly compiled from AFAD and ISC catalogues. The LET algorithm was used to identify three-dimensional velocity variations in the crust that are mostly related to lithological and petrological properties of the different geological units. The Aliaga (AGS), Seferihisar (SGS), and Urla (UHS) regions are represented by low V_p/V_s, low V_p which are in agreement with previous studies performed in different regions. A similar observation is found for the Cesme (CGS) area, but the results are less reliable due to the insufficient number of earthquakes. The gas-filled porosity would result in low V_p, low V_s anomalies and a relatively low V_p/V_s ratio, as we concluded for the geothermal systems of Izmir. High V_p/V_s and low V_p indicate high fluid content beneath the Menemen (MGS) area. The Balcova geothermal system (BGS) exhibits complex V_p/V_s characteristics at different depths down to 15 km, suggesting different lithology. Velocity anomalies ranging down to 30 km reveal different depth layers. The upper crust mainly comprises Neogene sediments and Quaternary alluvial deposits showing low velocities. The middle layer exhibits velocities typical of the gabbro and other lithospheric crystalline rocks. A sharp increase in velocities is evident at the lower crustal layer revealing the Bornova Flysch zone. We report at 27 km of depth an undulated transition at the crustal-mantle boundary. Whether our tomographic results could be the starting point for further investigation, we report that P- and S-wave anomalies show a fairly good correlation between velocity patterns of the main structural and tectonic features available in the region. A slight increase in the crustal thickness is evident towards the north and east as derived from the cross-sections at depth. We find that past tectonic processes, such as large lateral offsets along the strike-slip faults and extensional tectonics, contribute some complexity and heterogeneity.

Acknowledgements. This study is a part of the Ph.D. thesis of Caglar Ozer at the Institute of Natural and Applied Sciences in DEU, Izmir, Turkey. This study is financed by DEU (Nr. 2016.KB.FEN.013). Data was downloaded from ISC (Thatcham, UK) and AFAD (Ankara, Turkey). We appreciate Ivan Koulakov for his continuous assistance during the preparation of the paper and for providing the latest modules of the local tomography software (LOTOS). We are grateful to the editor, Dario Slejko, for his rigorous and constructive criticisms, as well as two anonymous reviewers for their critical remarks, which helped us to improve the paper. All images (except Figs. 1 and 2) are generated using GMT (Wessel and Smith, 1998). Calculations were performed in the Seismological Laboratory (SeismoLab) belonging to the Geophysical Engineering Department of DEU.

REFERENCES

Akgun M., Gonenc T., Pamukcu O. and Ozyalin S.; 2014: *Investigation of the relationship between ground and engineering bedrock at northern part of the Gulf of Izmir by borehole data supported geophysical works*. J. Earth Syst. Sci., **123**, 545-564.

Akin A., Ulugergerli E.U. and Kutlu S.; 2014: *The assessment of geothermal potential of Turkey by means of heat flow estimation*. Bull. Mineral Res. Explor., **149**, 201-210, <bulletin.mta.gov.tr>.

Aksoy N., Serpen U. and Filiz S.; 2008: *Management of the Balcova-Narlidere geothermal reservoir, Turkey*. Geotherm., **37**, 444-466.

Aktug B. and Kilicoglu A.; 2006: *Recent crustal deformation of Izmir, western Anatolia and surrounding regions as deduced from repeated GPS measurements and strain field*. J. Geodyn., **41**, 471-484.

Aldanmaz E., Pearce J.A., Thirlwall M.F. and Mitchell J.G.; 2000: *Petrogenetic evolution of late Cenozoic, post-collision volcanism in western Anatolia, Turkey*. J. Volcanol. Geotherm. Res., **102**, 67-95.

Ates A., Kearey P. and Tufan S.; 1999: *New gravity and magnetic anomaly maps of Turkey*. Geophys. J. Int., **136**, 499-502.

Avsar U., Hubert-Ferrari A., Batist M.D. and Fagel N.; 2014a : *A 3400 year lacustrine paleoseismic record from the North Anatolian Fault, Turkey: implications for bimodal recurrence behavior*. Geophys. Res. Lett., **41**, 377-384.

Avsar U., Hubert-Ferrari A., Batist M.D., Lepoint G., Schmidt S. and Fagel N.; 2014b: *Seismically-triggered organic-rich layers in recent sediments from Lake Göllüköy (North Anatolian Fault, Turkey)*. Quat. Sci. Rev., **103**, 67-80.

Avsar U., Hubert-Ferrari A., Batist M.D., Schmidt S. and Fagel N.; 2015 : *Sedimentary records of past earthquakes in Boraboy Lake during the last ca 600 years (North Anatolian Fault, Turkey)*. Palaeogeogr. Palaeoclimatol. Palaeoecol., **433**, 1-9.

Avsar U., Jónsson S., Avsar O. and Schmidt S.; 2016: *Earthquake-induced soft-sediment deformations and seismically amplified erosion rates recorded in varved sediments of Koycegiz Lake (SW Turkey)*. J. Geophys. Res., **121,** 4767-4779.

Aydan O., Kumsar H. and Tano H.; 2005: *Multiparameter changes in the earth's crust and their relation to earthquakes in Denizli region of Turkey.* In: Proc. World Geotherm. Congr., Antalya, Turkey, pp. 1-10.

Aydin I., Karat H.I. and Kocak A.; 2005: *Curie-point depth map of Turkey*. Geophys. J. Int., **162**, 633-640.

Bakirci T., Yoshizawa K. and Ozer M.F.; 2012: *Three-dimensional S-wave structure of the upper mantle beneath Turkey from surface wave tomography*. Geophys. J. Int., **190**, 1058-1076.

Bekler T. and Gurbuz C.; 2008: *Insight into the crustal structure of the eastern Marmara Region, NW Turkey*. Pure Appl. Geophys., **165**, 295-309.

Bilim F., Akay T., Aydemir A. and Kosaroglu S.; 2016: *Curie point depth, heat-flow and radiogenic heat production deduced from the spectral analysis of the aeromagnetic data for geothermal investigation on the Menderes Massif and the Aegean Region, western Turkey*. Geotherm., **60**, 44-57.

Caglar I.; 2001: *Electrical resistivity structure of the northwestern Anatolia and its tectonic implications for the Sakarya and Bornova zones*. Phys. Earth Planet. Inter., **125**, 95-110.

Cambaz M.D. and Karabulut H.; 2010: *Love-wave group velocity maps of Turkey and surrounding regions*. Geophys. J. Int., **181**, 502-520.

Cevikbilen S.Y., Biryol C.B., Beck S., Zandt G., Taymaz T., Adiyaman H.E. and Ozacar A.A.; 2012: *3-D crustal structure along the North Anatolian Fault zone in north-central Anatolia revealed by local earthquake tomography*. Geophys. J. Int., **188**, 819-849.

Cisternas A., Polat O. and Rivera L.; 2004: *The Marmara Sea Region: seismic behaviour in time and the likelihood of another large earthquake near Istanbul (Turkey)*. J. Seismol., **8**, 427-437.

Coskun S., Dondurur D., Cifci G., Aydemir A. and Drahor M.G.; 2016: *Natural and anthropogenic submarine morphologies revealed by high resolution acoustic data in the Gulf of Izmir, western Turkey*. Mar. Pet. Geol., **71**, 211-224.

Delph J.R., Biryol C.B., Beck L.B., Zandt G. and Ward K.M.; 2015: *Shear wave velocity structure of the Anatolian Plate: anomalously slow crust in southwestern Turkey*. Geophys. J. Int., **202**, 261-276.

Dolmaz M.N., Hisarli Z.M., Ustaomer T. and Orbay N.; 2005: *Curie point depths based on spectrum analysis of aeromagnetic data, west Anatolian extensional province, Turkey*. Pure Appl. Geophys., **162**, 571-590.

Drahor M.G. and Berge A.M.; 2006: *Geophysical investigations of the Seferihisar geothermal area, western Anatolia, Turkey*. Geotherm., **35**, 302-320.

Duzgit Z., Hisarli Z.M., Sayin N. and Orbay N.; 2006: *Correlation between gravity and magnetic anomalies of western Anatolia and its relation to tectonic structures*. Earth, Planets Space, **58**, 943-949.

Emre O. and Ozalp S.; 2011: *1:250,000 scale new active fault map of Turkey, Urla (NJ 35-6) Quadrangle*. General Directorate of Mineral Research and Exploration, Serial n. 5, Ankara, Turkey.

Erkan K.; 2015: *Geothermal investigations in western Anatolia using equilibrium temperatures from shallow boreholes*. Solid Earth, **6**, 103-113.

Ersoy E.Y., Helvaci C., Sozbilir H., Erkul F. and Bozkurt E.; 2008: *A geochemical approach to Neogene-Quaternary volcanic activity of western Anatolia: an example of episodic bimodal volcanism within the Selendi Basin, Turkey*. Chem. Geol., **255**, 265-282.

Ersoy E.Y., Helvaci C. and Palmer M.R.; 2010: *Mantle source characteristics and melting models for the early-middle Miocene mafic volcanism in western Anatolia: implications for enrichment processes of mantle lithosphere and origin of K-rich volcanism in post-collisional settings*. J. Volcanol. Geotherm. Res., **198**, 112-128.

Ersoy E.Y., Cemen I., Helvaci C. and Billor Z.; 2014: *Tectono-stratigraphy of the Neogene basins in western Turkey: implications for tectonic evolution of the Aegean Extended Region*. Tectonophys., **635**, 33-58.

Frederiksen A.W., Thompson D.A., Rost S., Cornwell D.G., Gulen L., Houseman G.A., Kahraman M., Poyraz S.A., Teoman U.M., Turkelli N. and Utkucu M.; 2015: *Crustal thickness variations and isostatic disequilibrium across the North Anatolian Fault, western Turkey*. Geophys. Res. Lett., **42**, 751-757.

Genc S.C., Altunkaynak S., Karacik Z. and Yilmaz Y.; 2001: *The Cubukludag Graben, Karaburun Peninsula: its tectonic significance in the Neogene geological evolution of the western Anatolia*. Geodin. Acta, **14**, 45-55.

Gessner K., Ring U., Christopher J., Hetzel R., Passchier C.W. and Gungor T.; 2001: *An active bivergent rolling-hinge detachment system: central Menderes metamorphic core complex in western Turkey*. Geol., **29**, 611-614.

Gessner K., Gallardo L.A., Markwitz V., Ring U. and Thomson S.N.; 2013: *What caused the denudation of the Menderes Massif: review of crustal evolution, lithosphere structure and dynamic topography in southwest Turkey*. Gondwana Res., **24**, 243-274.

Gok E. and Polat O.; 2012: *An assessment of the seismicity of the Bursa Region from a temporary seismic network*. Pure Appl. Geophys., **169**, 659-675.

Gok E. and Polat O.; 2014: *An assessment of the microseismic activity and focal mechanisms of the Izmir (Smyrna) area from a new local network, IzmirNET*. Tectonophys., **635**, 154-164.

Gok E., Chavez-Garcia F.J. and Polat O.; 2014 : *Effect of soil conditions on predicted ground motion: case study from western Anatolia, Turkey*. Phys. Earth Planet. Inter., **229**, 88-97.

Gurbuz C., Aktar M., Eyidogan H., Cisternas A., Haessler H., Barka A., Ergin M., Turkelli N., Polat O., Ucer S.B., Kuleli S., Baris S., Kaypak B., Bekler T., Zor E., Bicmen F. and Yoruk A.; 2000: *On seismotectonics of the Marmara* region *(Turkey): results from a microseismic experiment*. Tectonophys., **316**, 1-17.

Gurbuz C., Bekler T., Toksoz M.N., Kuleli S., Kalafat D. and Schultz C.A.; 2003: *Seismic refraction studies and crustal structure in Anatolia*. In: 12th International Workshop, Commission on controlled-source seismology: deep seismic methods, Mountain Lake, VA, USA, <www.geophys.geos.vt.edu/hole/ccss/gurbuzCCSS.pdf>.

Gurer A. and Bayrak M.; 2007: *Relation between electrical resistivity and earthquake generation in the crust of west Anatolia, Turkey*. Tectonophys., **445**, 49-65.

Gurer A., Bayrak M., Gurer O.F. and Ilkisik O.M.; 2004: *The deep resistivity structure of southwestern Turkey: tectonic implications*. Int. Geol. Rev., **46**, 655-670.

Hauksson E.; 2000: *Crustal structure and seismicity distribution adjacent to the Pacific and North America Plate boundary in southern California*. J. Geophys. Res., **105**, 13875-13903.

Helvaci C., Ersoy E.Y., Sozbilir H., Erkul F., Sumer O. and Uzel B.; 2009: *Geochemistry and 40Ar/39Ar geochronology of Miocene volcanic rocks from the Karaburun Peninsula: implications for amphibole-bearing lithospheric mantle source, western Anatolia*. J. Volcanol. Geotherm. Res., **185**, 181-202.

Hosny A., El-Hady S., El-Ela A.M.A., Panza G.F., Tealeb A. and El Rahman M.A.; 2009: *Magma intrusion in the upper crust of the Abu Dabbab area, southeast of Egypt from Vp and Vp/Vs tomography*. Rendiconti Lincei, **20**, 1-19.

Ilkisik O.M.; 1995: *Regional heat flow in western Anatolia using silica temperature estimates from thermal springs*. Tectonophys., **244**, 175-184.

Inan S., Ergintav S., Saatcilar R., Tuzel B. and Iravul Y.; 2007: *Turkey makes major investment in earthquake research*. EOS Trans. Am. Geophys. Union, **88**, 333-334.

International Seismological Centre; 2003: *On-line ISC Bulletin*. Thatcham, United Kingdom, <www.isc.ac.uk>.

Jaxybulatov K., Koulakov I., Ibs-von Seht M., Klinge K., Reichert C., Dahren B. and Troll V.R.; 2011: *Evidence for high fluid/melt content beneath Krakatau Volcano (Indonesia) from local earthquake tomography*. J. Volcanol. Geotherm. Res., **206**, 96-105.

Jolivet L., Faccenna C. and Huet B.; 2013: *Aegean tectonics: strain localisation, slab tearing and trench retreat*. Tectonophys., **597-598**, 1-33.

Kaftan I., Salk M. and Senol Y.; 2011: *Evaluation of gravity data by using artificial neural networks case study: Seferihisar geothermal area (western Turkey)*. J. Appl. Geophys., **75**, 711-718.

Kaftan I., Sindirgi P. and Akdemir O.; 2014: *Inversion of self potential anomalies with multilayer perceptron neural networks*. Pure Appl. Geophys., **171**, 1939-1949.

Kahraman M., Cornwell D.G., Thompson D.A., Rost S., Houseman G.A., Turkelli N., Teoman U., Poyraz A.S., Utkucu M. and Gulen L.; 2015: *Crustal-scale shear zones and heterogeneous structure beneath the North Anatolian Fault Zone, Turkey, revealed by a high-density seismometer array.* Earth Planet. Sci. Lett., **430**, 129-139.

Karabulut H., Paul A., Ergun T.A., Hatzfeld D., Childs D.M. and Aktar M.; 2013: *Long-wavelength undulations of the seismic Moho beneath the strongly stretched western Anatolia*. Geophys. J. Int., **194**, 450-464.

Kaya C.; 2010: *Deep crustal structure of northwestern part of Turkey*. Tectonophys., **489**, 227-239.

Kaypak B.; 2008: *Three-dimensional Vp and Vp/Vs structure of the upper crust in the Erzincan Basin (eastern Turkey)*. J. Geophys. Res., **113**, 1-20.

Kaypak B. and Gokkaya G.; 2012: *3-D imaging of the upper crust beneath the Denizli geothermal* region *by local earthquake tomography, western Turkey*. J. Volcanol. Geotherm. Res., **211-212**, 47-60.

Kececioglu M., Polat O., Gok E., Ceken U. and Chavez-Garcia F.J.; 2012: *Cross-correlation of ambient noise: example from Izmir Metropolitan City, Turkey.* In: Proc. 33rd European Seismological Commission, Moscow, Russia, p. 271.

Khrepy S., Koulakov I. and Arifi N.; 2015: *Crustal structure in the area of the Cannon Earthquakes of Abu Dabbab (northern Red Sea, Egypt), from seismic tomography inversion*. Bull. Seismol. Soc. Am., **105**, 1870-1882.

Komut T., Gray R., Pysklywec R. and Gogus O.H.; 2012: *Mantle flow uplift of western Anatolia and the Aegean: interpretations from geophysical analyses and geodynamic modelling*. J. Geophys. Res., **117,** B11412, doi:10.1029/2012|B009306.

Koulakov I.; 2009: *LOTOS code for local earthquake tomographic inversion: bench-marks for testing tomographic algorithms*. Bull. Seismol. Soc. Am., **99**, 194-214.

Koulakov I., Yudistira T., Luehr B.G. and Wandono; 2009: *P, S velocity and Vp/Vs ratio beneath the Toba caldera complex (northern Sumatra) from local earthquake tomography*. Geophys. J. Int., **177**, 1121-1139.

Koulakov I., Bindi D., Parolai S., Grosser H. and Milkereit C.; 2010a: *Distribution of seismic velocities and attenuation in the crust beneath the North Anatolian Fault (Turkey) from local earthquake tomography*. Bull. Seismol. Soc. Am., **100**, 207-224.

Koulakov I., Zaharia B., Enescu B., Radulian M., Popa M., Parolai S. and Zschau J.; 2010b: *Delamination or slab detachment beneath Vrancea ? New arguments from local earthquake tomography*. Geochem. Geophys. Geosyst., **11**, 1-24.

Lees J.M. and Wu H.; 1999: *P wave anisotropy, stress, and crack distribution at Coso geothermal field, California*. J. Geophys. Res., **104**, 17955-17973.

Magri F., Akar T., Gemici U. and Pekdeger A.; 2010: *Deep geothermal groundwater flow in the Seferihisar-Balcova area, Turkey: results from transient numerical simulations of coupled fluid flow and heat transport processes*. Geofluids, **10**, 388-405.

Magri F., Akar T., Gemici U. and Pekdeger A.; 2012: *Numerical investigations of fault-induced seawater circulation in the Seferihisar-Balvova Geothermal system, western Turkey*. Hydrogeol. J., **20**, 103-118.

Muksin U., Bauer K. and Haberland C.; 2013: *Seismic Vp and Vp/Vs structure of the geothermal area around Tarutung (north Sumatra, Indonesia) derived from local earthquake tomography*. J. Volcanol. Geotherm. Res., **260**, 27-42.

Mutlu A.K. and Karabulut H.; 2011: *Anisotropic Pn tomography of Turkey and adjacent regions*. Geophys. J. Int., **187**, 1743-1758.

Nolet G.; 1990: *Partitioned waveform inversion and two-dimensional structure under the network of autonomously recording seismograph*. J. Geophys. Res., **95**, 8499-8512.

Okay A.I. and Altiner D.; 2007: *A condensed Mesozoic succession north of Izmir: a fragment of the Anatolide-Tauride Platform in the Bornova Flysch Zone*. Turk. J. Earth Sci., **16**, 257-279.

Oner Z. and Dilek Y.; 2011: *Supradetachment basin evolution during continental extension: the Aegean province of western Anatolia, Turkey*. Bull. Geol. Soc. Am., **123**, 2115-2141.

Ozener H., Dogru A. and Acar M.; 2013: *Determination of the displacements along the Tuzla Fault (Aegean region - Turkey): preliminary results from GPS and precise levelling techniques*. J. Geodyn., **67**, 13-20.

Ozer C. and Polat O.; 2016a: *Seismic underground characteristics beneath Izmir geothermal area*. In: International Workshop on Earthquakes in north Iceland, Husavik, Iceland, pp. 57-59, <www.hac.is/rannsoknir/earthquake-husavik2016>.

Ozer C. and Polat O.; 2016b: *3-D tomographic modelling beneath Izmir geothermal area*. In: Abstracts International Geothermal Congress, Izmir, Turkey, <igc-turkey.com/#speakers>.

Ozer C. and Polat O.; 2017: *Determination of 1-D (One-Dimensional) seismic velocity structure of Izmir and surroundings*. J. Sci. Eng., Dokuz Eylul University, **19**, 147-168, <web.deu.edu.tr/fmd/sayi55.htm>.

Ozguler M.E. and Unay T.; 1977: *Resistivity field work for exploration of geothermal energy in Seferihisar, Izmir, Turkey.* In: Proc. Symposium Geothermal Energy, Ankara, Turkey, pp. 115-130.

Ozkan R., Sener M., Helvaci C. and Sener M.F.; 2011: *Hydrothermal alterations and relationship with thermal waters at Aliaga (Izmir) geothermal field*. Bull. Earth Sci., **32**, 1-20, <www.yerbilimleri.hacettepe.edu.tr>.

Ozmen B. and Can H.; 2016: *Ankara icin deterministik deprem Tehlike analizi*. J. Fac. Eng. Archit. Gazi Univ., **31**, 9-18.

Paige C.C. and Saunders M.A.; 1982: *LSQR: an algorithm for sparse linear equations and sparse least squares*. ACM Trans. Math. Softw., **8**, 43-71.

Pamukcu O. and Yurdakul A.; 2008: *Isostatic compensation in western Anatolia with estimate of the effective elastic thickness*. Turk. J. Earth Sci., **17**, 545-557.

Pamukcu O., Gonenc T., Uyanik O., Sozbilir H. and Cakmak O.; 2014: *A microgravity model for the city of Izmir (western Anatolia) and its tectonic implementations*. Acta Geophys., **62**, 849-871.

Pamukcu O., Gonenc T., Cirmik A. and Kahveci M.; 2015a: *Investigation of the Sigacik Bay's displacement characteristic by using GPS and gravity data in western Anatolia*. J. Asian Earth Sci., **99**, 72-84.

Pamukcu O., Gonenc T., Cirmik A., Sindirgi P., Kaftan I. and Akdemir O.; 2015b: *Investigation of vertical mass changes in the south of Izmir (Turkey) by monitoring microgravity and GPS/GNSS methods*. J. Earth Syst. Sci., **124**, 137-148.

Paul A., Karabulut H., Mutlu A.K. and Salaun G.; 2014: *A comprehensive and densely sampled map of shear-wave azimuthal anisotropy in the Aegean-Anatolia region*. Earth Planet. Sci. Lett., **389**, 14-22.

Polat O., Haessler H., Cisternas A., Philip H., Eyidogan H., Aktar M., Frogneux M., Comte D. and Gurbuz C.; 2002a: *The Izmit (Kocaeli) Turkish earthquake of August 17, 1999: previous seismicity, aftershocks and seismotectonics*. Bull. Seismol. Soc. Am., **92**, 361-375.

Polat O., Haessler H., Cisternas A., Philip H. and Eyidogan H.; 2002b: *Analysis and interpretation of the aftershock sequence of the August 17, 1999, Izmit (Turkey) earthquake*. J. Seismol., **6**, 287-306.

Polat O., Gok E. and Yilmaz D.; 2008: *Earthquake Hazard of the Aegean Extension Region (west Turkey)*. Turk. J. Earth Sci., **17**, 593-614.

Polat O., Ceken U., Uran T., Gok E., Yilmaz N., Beyhan M., Koc N., Arslan B., Yilmaz D. and Utku M.; 2009: *IzmirNet: a strong-motion network in metropolitan Izmir, western Anatolia, Turkey*. Seismol. Res. Lett., **80**, 831-838.

Poyraz S.A., Teoman M.U., Turkelli N., Kahraman M., Cambaz D., Mutlu A., Rost S., Houseman G.A., Thompson D.A., Cornwell D., Utkucu M. and Gulen L.; 2015: *New constraints on micro-seismicity and stress state in the western part of the North Anatolian Fault Zone: observations from a dense seismic array*. Tectonophys., **656**, 190-201.

Reilinger R., McClusky S., Paradissis D., Ergintav S. and Vernant P.; 2010: *Geodetic constraints on the tectonic evolution of the Aegean* region *and strain accumulation along the Hellenic subduction zone*. Tectonophys., **488**, 22-30.

Sahin S. and Cinar M.; 2014: *Frequency-dependent attenuation of coda waves in the crust in southwest Anatolia (Turkey)*. Pure Appl. Geophys., **171**, 1203-1217.

Sahin S., Bao X., Turkelli N., Sandvol E., Teoman U. and Kahraman M.; 2013: *Lg wave attenuation in the Isparta Angle and Anatolian Plateau (Turkey)*. Pure Appl. Geophys., **170**, 337-351.

Salah M.K., Sahin S. and Destici C.; 2007: *Seismic velocity and Poisson's ratio tomography of the crust beneath southwest Anatolia: an insight into the occurrence of large earthquakes*. J. Seismol., **11**, 415-432.

Salah M.K., Sahin S. and Topatan U.; 2014: *Crustal velocity and Vp/Vs structures beneath central Anatolia from local seismic tomography*. Arabian J. Geosci., **7**, 4101-4118.

Salaun G., Pedersen H.A., Paul A., Farra V., Karabulut H., Hatzfeld D., Papazachos C., Childs D.M., Pequegnat C. and SIMBAAD Team; 2012: *High-resolution surface wave tomography beneath the Aegean-Anatolia region: constraints on upper-mantle structure*. Geophys. J. Int., **190**, 406-420.

Salk M., Pamukcu O. and Kaftan I.; 2005: *Determination of the Curie point depth and heat flow from Magsat data of western Anatolia*. J. Balkan Geophys. Soc., **8**, 149-160.

Serpen U., Aksoy N., Ongur T. and Korkmaz E.D.; 2009: *Geothermal energy in Turkey: 2008 update*. Geotherm., **38**, 227-237.

Serrano I., Zhao D. and Morales J.; 2002: *3-D crustal structure of the extensional Granada Basin in the convergent boundary between the Eurasian and African plates*. Tectonophys., **344**, 61-79.

Shater A.B.A.; 2012: *Earthquakes relocation in three-dimension P-wave velocity model for Abu Dabbab area, Red Sea, Egypt*. Middle-East J. Sci. Res., **12**, 796-800.

Sherburn S., Bannister S. and Bibby H.; 2003: *Seismic velocity structure of the central Taupo Volcanic Zone, New Zealand, from local earthquake tomography*. J. Volcanol. Geotherm. Res., **122**, 69-88.

Sindirgi P., Pamukcu O. and Ozyalin S.; 2008: *Application of normalized full gradient method to self potential (SP) data*. Pure Appl. Geophys., **165**, 409-427.

Sufri O., DeShon H.R., Scales M., Hayward C., Magnani M.B. and Hornbach M.; 2016: *Imaging crustal structure using local earthquake and ambient noise tomography in north Texas*. In: Abstract, Fall Meeting, Am. Geophys. Union, San Francisco, CA, USA.

Tarcan G., Gemici U. and Aksoy N.; 2005: *Hydrogeological and geochemical assessments of the Gediz Graben geothermal areas, western Anatolia, Turkey*. Environ. Geol., **47**, 523-534.

Tarcan G., Gemici U. and Aksoy N.; 2009: *Hydrogeochemical factors effecting the scaling problem in Balcova geothermal field Izmir, Turkey*. Environ. Geol., **58**, 1375-1386.

Tezel T., Shibutani T. and Kaypak B.; 2010: *Crustal structure variation in western Turkey inferred from the receiver function analysis*. Tectonophys., **492**, 240-252.

Tezel T., Shibutani T. and Kaypak B.; 2013: *Crustal thickness of Turkey determined by receiver function*. J. Asian Earth Sci., **75**, 36-45.

Totaro C., Koulakov I., Orecchio B. and Presti D.; 2014: *Detailed crustal structure in the area of the southern Apennines-Calabrian Arc border from local earthquake tomography*. J. Geodyn., **82**, 87-97.

Tunc B.; 2008: *Determination of three-dimensional velocity structure of Marmara region using seismic tomography method*. Ph.D. Thesis in Natural and Applied Sciences, The Graduate School, Kocaeli University, Turkey.

Tunc B., Caka D., Irmak T.S., Woith H., Tunc S., Baris S., Ozer M.F., Luhr B.G., Gunther E., Grosser H. and Zschau J.; 2011: *The Armutlu network: an investigation into the seismotectonic setting of Armutlu-Yalova-Gemlik and the surrounding regions*. Ann. Geophys., **54**, 35-45.

Ustaszewski K., Wu Y.M., Suppe J., Huang H.H., Chang C.H. and Carena S.; 2012: *Crust-mantle boundaries in the Taiwan-Luzon arc-continent collision system determined from local earthquake tomography and 1D models: implications for the mode of subduction polarity reversal*. Tectonophys., **578**, 31-49.

Uzel B., Sozbilir H. and Ozkaymak C.; 2012: *Neotectonic evolution of an actively growing superimposed basin in western Anatolia: the Inner Bay of Izmir, Turkey*. Turk. J. Earth Sci., **21**, 439-471.

Uzel B., Sozbilir H., Ozkaymak C., Kaymakci N. and Langereis C.G.; 2013: *Structural evidence for strike-slip deformation in the Izmir-Balikesir transfer zone and consequences for late Cenozoic evolution of western Anatolia (Turkey)*. J. Geodyn., **65**, 94-116.

Wessel P. and Smith W.H.L.; 1998: *New version of the generic mapping tools released*. EOS Trans. Am. Geophys. Union, **79**, 579.

Xu Y., Koper K.D., Sufri O., Zhu L. and Hutko A.R.; 2009: *Rupture imaging of the Mw 7.9 12 May 2008 Wenchuan earthquake from back projection of teleseismic P waves*. Geochem. Geophys. Geosyst., **10**, 1-17.

Yilmazer S. and Alacali M.; 2005: *Distribution of hot water resources and potentials of Izmir province*. In: Proc. World Geothermal Congress, Antalya, Turkey, <www.geothermal-energy.org/pdf/IGAstandard/WGC/2005/2325.pdf>.

Yin A.; 2010: *Cenozoic tectonic evolution of Asia: a preliminary synthesis*. Tectonophys., **488**, 293-325.

Corresponding author: Polat Orhan
Division of Seismology, Department of Geophysics, Engineering Faculty, Dokuz Eylul University (DEU)
Izmir 35160, Turkey
Phone: +90 232 3017266; fax: +90 232 4538366; e-mail:orhan.polat@deu.edu.tr.